catalysts

MDPI

Article

Novel Highly Efficient Green and Reusable Cu(II)/Chitosan-Based Catalysts for the Sonogashira, Buchwald, Aldol, and Dipolar Cycloaddition Reactions

Artem P. Dysin [1], Anton R. Egorov [1], Omar Khubiev [1], Roman Golubev [2], Anatoly A. Kirichuk [1], Victor N. Khrustalev [1], Nikolai N. Lobanov [1], Vasili V. Rubanik [2], Alexander G. Tskhovrebov [1] and Andreii S. Kritchenkov [1,2,*]

[1] Faculty of Science, Peoples' Friendship University of Russia (RUDN University), Moscow 117198, Russia
[2] Metal Physics Laboratory, Institute of Technical Acoustics NAS of Belarus, 210009 Vitebsk, Belarus
* Correspondence: kritchenkov-as@rudn.ru

Abstract: In this study, new Cu(II)/chitosan-based systems were designed via (i) the treatment of chitosan with sodium sulfate (**1a**) or sodium acetate (**1b**); (ii) the coating of **1a** or **2a** with a sodium hyaluronate layer (**2a** and **2b**, correspondingly); (iii) the treatment of a cholesterol–chitosan conjugate with sodium sulfate (**3a**) or sodium acetate (**3b**); and (iv) the succination of **1a** and **1b** to afford **4a** and **4b** or the succination of **2a** and **2b** to yield **5a** and **5b**. The catalytic properties of the elaborated systems in various organic transformations were evaluated. The use of copper sulfate as the source of Cu^{2+} ions results in the formation of nanoparticles, while the use of copper acetate leads to the generation of conventional coarse-grained powder. Cholesterol-containing systems have proven to be highly efficient catalysts for the cross-coupling reactions of different types (e.g., Sonogashira, Buchwald–Hartwig, and Chan–Lam types); succinated systems coated with a layer of hyaluronic acid are promising catalysts for the aldol reaction; systems containing inorganic copper(II) salt nanoparticles are capable of catalyzing the nitrile-oxide-to-nitrile 1,3-dipolar cycloaddition. The elaborated catalytic systems efficiently catalyze the aforementioned reactions in the greenest solvent available, i.e., water, and the processes could be conducted in air. The studied catalytic reactions proceed selectively, and the isolation of the product does not require column chromatography. The product is separated from the catalyst by simple filtration or centrifugation.

Keywords: chitosan; copper; nanoparticles; green catalysis; Sonogashira reaction; Buchwald reaction; aldol reaction; dipolar cycloaddition

Citation: Dysin, A.P.; Egorov, A.R.; Khubiev, O.; Golubev, R.; Kirichuk, A.A.; Khrustalev, V.N.; Lobanov, N.N.; Rubanik, V.V.; Tskhovrebov, A.G.; Kritchenkov, A.S. Novel Highly Efficient Green and Reusable Cu(II)/Chitosan-Based Catalysts for the Sonogashira, Buchwald, Aldol, and Dipolar Cycloaddition Reactions. *Catalysts* **2023**, *13*, 203. https://doi.org/10.3390/catal13010203

Academic Editors: Monica Nardi, Svilen P. Simeonov and Herrera Cano Natividad Carolina

Received: 30 November 2022
Revised: 5 January 2023
Accepted: 10 January 2023
Published: 15 January 2023

1. Introduction

The ever increasing demand for environmentally friendly processes and materials from both basic science and industry has significantly promoted the research of chitosan as a component of catalytic systems (for example, as a polymeric support or as a fully organic active component) [1,2]. The ever-increasing number of highly cited publications in this field indeed testifies to the importance of this direction and the great deal of interest in it. Chitosan is one of the most abundant natural polymers, and it is characterized by prominent biodegradability and biocompatibility [3].

Chitosan can be employed as a catalyst in various organic transformations; however, the scope of these reactions is strongly limited by the simplest reactions such as carbonyl compounds condensation [2].

Recently, our scientific group has developed a number of chitosan-based catalytic systems [4–9]. However, although the systems are very efficient, they require sophisticated and laborious preparation. Facile catalytic systems are undoubtedly more advantageous and are of much greater interest.

On the other hand, there are several reports in the literature on the efficiency of copper ions in the catalysis of organic transformations [10–14]. Copper ions can be considered as universal catalysts for important C–C, C–O, and C–N bond formation and a number of multicomponent reactions and domino reactions, including those leading to the formation of complex heterocyclic systems. Progress in this area has been extensively discussed in recent reviews [15–21]. These prominent examples also include copper ions as a component of chitosan-based systems [22–24]. However, we failed to find any studies in the literature in which a number of structurally related simple catalytic chitosan-based systems containing copper ions were tested as catalysts towards various types of organic reactions. Furthermore, such studies are of high value, since they are the first and necessary step towards understanding the so-called "structure—catalytic activity relationships", which are of fundamental scientific importance. In the current study, we intended to prepare various structurally related catalytic systems based on chitosan and Cu(II). The mentioned systems were obtained according to the approaches described below:

(i) By simple treatment of chitosan by Cu(II) sulfate or Cu(II) acetate as sources of Cu^{2+} ions (Figure 1, **1a**, **1b**; Table 1, **1**–**6**);
(ii) By coating of **1**–**6** with a layer of hyaluronate-Na (Figure 1, **2a, 2b**; Table 1, **7**–**12**);
(iii) By the treatment of a cholesterol–chitosan conjugate by Cu(II) sulfate or Cu(II) acetate as sources of Cu^{2+} ions (Figure 1, **3a, 3b**; Table 1, **13**–**18**);
(iv) By the succination of **1**–**12** with succinic anhydride (Figure 1, **4a, 4b, 5a, 5b**; Table 1, **19**–**30**).

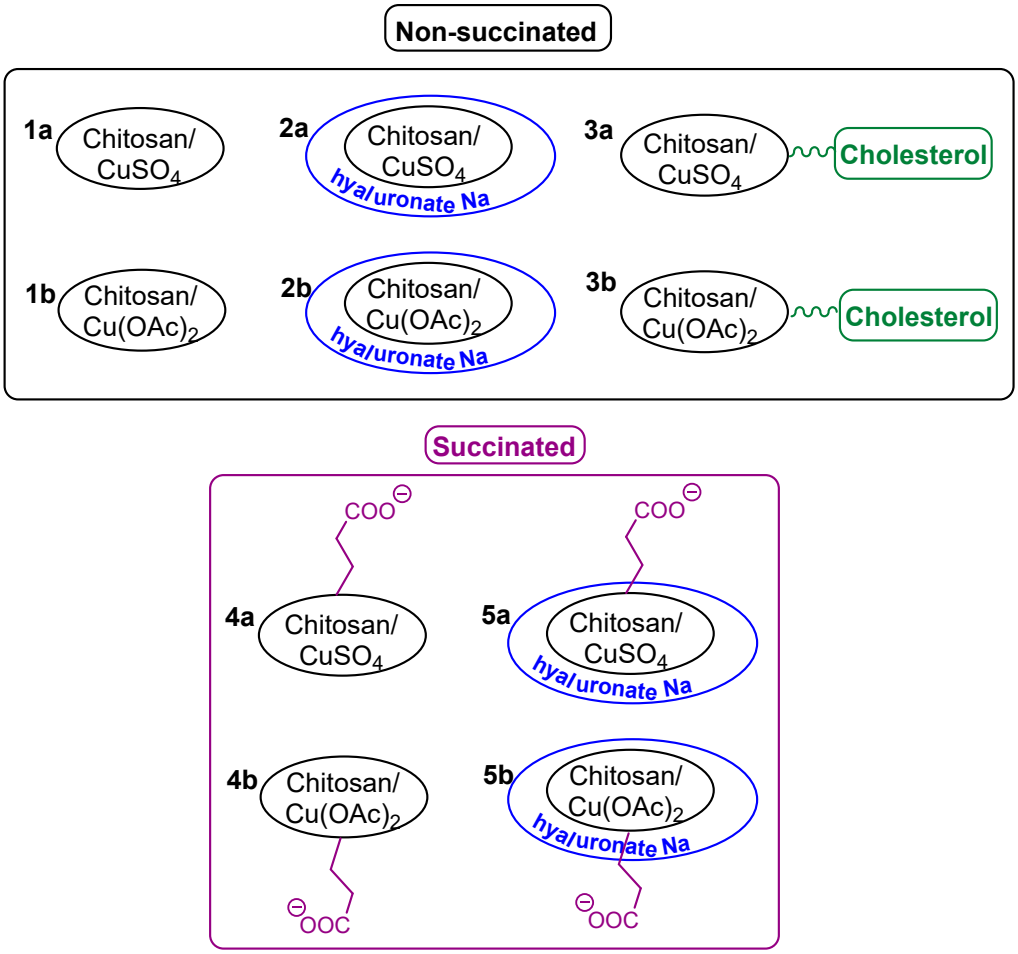

Figure 1. The systems under study.

Table 1. The elaborated chitosan/copper(II) composites and their characteristics.

	Composition of the Sample	No.	Size (nm)	Zeta-Potential (mV)	Copper(II) Content (%)	T_{onset} (°C)
Non-succinated	CS_{12}+$CuSO_4$	**1**	307	13.98 ± 0.32	17.4	205
	CS_{200}+$CuSO_4$	**2**	266	14.16 ± 0.13	18.1	202
	CS_{500}+$CuSO_4$	**3**	286	14.07 ± 0.14	17.7	207
	CS_{12}+CuOAc	**4**	-	-	13.3	157
	CS_{200}+CuOAc	**5**	-	-	13.8	168
	CS_{500}+CuOAc	**6**	-	-	13.6	182
	CS_{12}+$CuSO_4$+NaHA	**7**	329	7.08 ± 0.10	13.2	200
	CS_{200}+$CuSO_4$+NaHA	**8**	271	7.03 ± 1.12	13.0	205
	CS_{500}+$CuSO_4$+NaHA	**9**	288	7.37 ± 0.07	13.0	206
	CS_{12}+CuOAc+NaHA	**10**	-	-	8.3	177
	CS_{200}+CuOAc+NaHA	**11**	-	-	8.5	184
	CS_{500}+CuOAc+NaHA	**12**	-	-	8.7	186
	CS_{12}Chol+$CuSO_4$	**13**	99	8.22 ± 0.17	15.7	202
	CS_{200}Chol+$CuSO_4$	**14**	108	8.55 ± 0.15	15.7	201
	CS_{500}Chol+$CuSO_4$	**15**	93	8.37 ± 0.21	15.5	202
	CS_{12}Chol+CuOAc	**16**	-	-	10.9	185
	CS_{200}Chol+CuOAc	**17**	-	-	10.4	174
	CS_{500}Chol+CuOAc	**18**	-	-	10.6	181
Succinated	CS_{12}+$CuSO_4$	**19**	287	−4.14 ± 0.22	10.1	167
	CS_{200}+$CuSO_4$	**20**	271	−4.62 ± 0.10	10.0	161
	CS_{500}+$CuSO_4$	**21**	290	−4.23 ± 0.17	10.0	169
	CS_{12}+CuOAc	**22**	-	-	7.4	161
	CS_{200}+CuOAc	**23**	-	-	7.6	164
	CS_{500}+CuOAc	**24**	-	-	7.7	163
	CS_{12}+$CuSO_4$+NaHA	**25**	315	−21.06 ± 0.11	8.3	175
	CS_{200}+$CuSO_4$+NaHA	**26**	276	−21.18 ± 0.15	8.4	-
	CS_{500}+$CuSO_4$+NaHA	**27**	283	−20.88 ± 0.18	8.2	-
	CS_{12}+CuOAc+NaHA	**28**	315	−21.12 ± 0.30	5.6	-
	CS_{200}+CuOAc+NaHA	**29**	284	−20.66 ± 0.14	5.8	-
	CS_{500}+CuOAc+NaHA	**30**	303	−20.74 ± 0.21	5.8	-

Further, we intended to evaluate the catalytic activity of these systems in the greenest solvent available, i.e., water, towards a series of essential organic transformations: cross-coupling reactions (Sonogashira, Buchwald–Hartwig, and Chan–Lam), the aldol reaction, and nitrile-oxide-to-nitrile 1,3-dipolar cycloaddition. Our findings and experimental details are discussed in the sections below.

2. Results and Discussion

2.1. Preparation and Characterization of Chitosan/Copper(II) Composites

2.1.1. Preparation of Chitosan/Copper(II) Composites

The elaborated chitosan/copper(II) composites **1**–**30** are presented in Table 1. The simplest composites **1**–**6** were obtained by the conventional addition of a chitosan solution to copper(II) sulfate (for **1**–**3**) or copper(II) acetate (for **4**–**6**) solutions. Composites **7**–**12** were prepared from **1**–**6** by their coating with sodium hyaluronate. Composites **13**–**18** were synthesized by the treatment of a cholesterol–chitosan conjugate by copper(II) sulfate (for **13**–**15**) or copper(II) acetate (for **16**–**18**) solutions. The cholesterol–chitosan conjugate, in its turn, was prepared by the treatment of chitosan with succinyl cholesterol in the presence of EDC and NHS (the so-called carbodiimide method [25,26], Scheme 1).

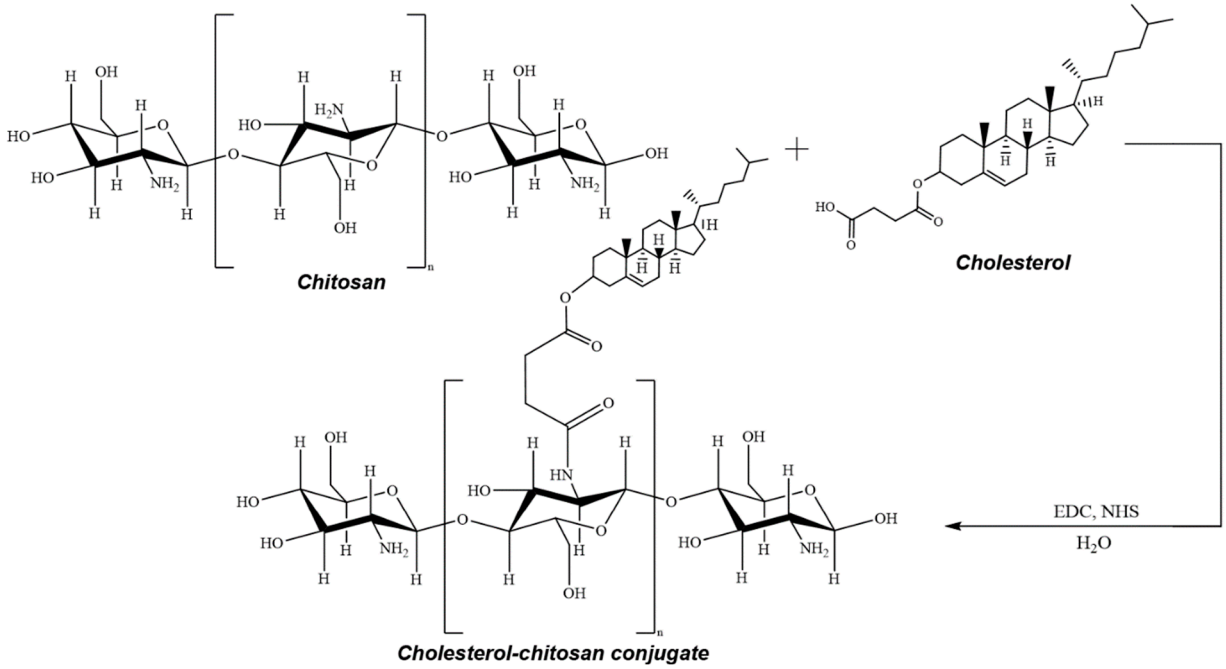

Scheme 1. The synthesis of the cholesterol–chitosan conjugate (CS—chitosan, Chol—cholesterol, CH-Chol—cholesterol–chitosan conjugate).

The treatment of the amino groups of the chitosan moieties in **1**–**12** by succinic anhydride (Scheme 2, [27]) resulted in succinated chitosan/copper(II)-based systems **19**–**30** (the degree of succination was ca. 20%, as confirmed by elemental analysis).

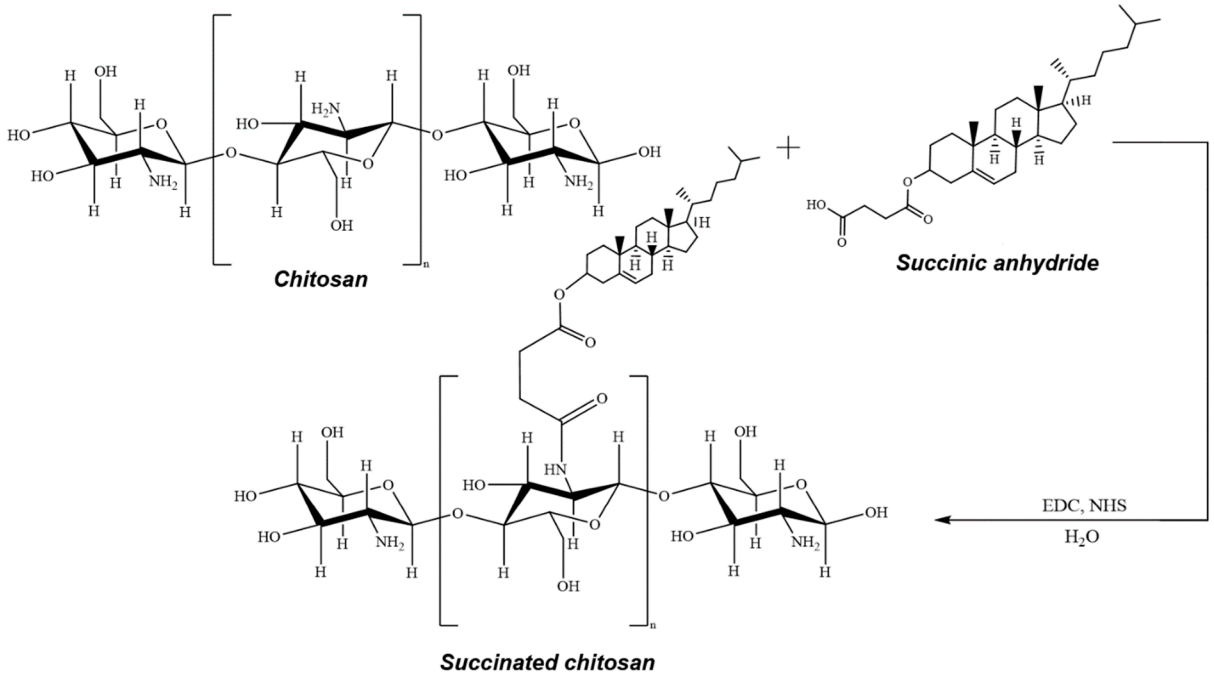

Scheme 2. The succination of the NH_2 groups of chitosan (CS—chitosan, Suc—succinic anhydride, CH-Suc—succinated chitosan).

Unfortunately, the treatment of **13**–**18** by succinic anhydride did not lead to their smooth succination, but rather to their destruction with the release of copper(II) ions. Thus, succinated analogues of **13**–**18** were prevented from being prepared.

2.1.2. Characterization of the Chitosan/Copper(II) Composites

Form of the Samples

The composites **1**–**3**, **7**–**9**, **13**–**15**, **19**–**21**, and **25**–**30** were in the form of particles of submicron size. Their sizes and ζ-potentials are presented in Table 1. The particles were of spherical shape, and this was confirmed by SEM (as an example, see Figure 2).

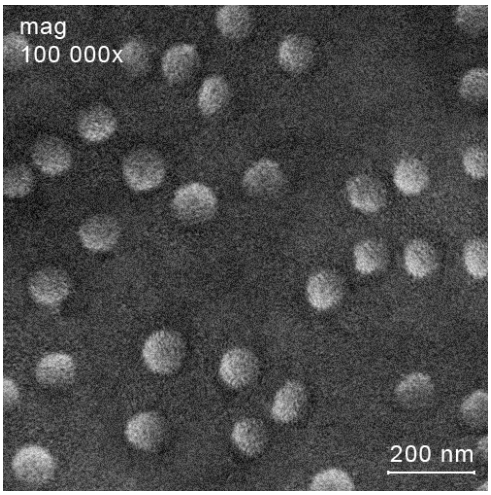

Figure 2. SEM image of **15**.

In chitosan chemistry, particles of such sizes are commonly referred to as nanoparticles [28]. Thus, we refer to **1**–**3**, **7**–**9**, **13**–**15**, **19**–**21**, and **25**–**30** composites as nanoparticles hereinafter in this paper. All other samples (**4**–**6**, **10**–**12**, **16**–**18**, and **22**–**24**) were obtained as coarse-grained powder not prone to the formation of nanoparticles.

X-ray Diffraction Study

The X-ray diffraction patterns of **1**–**12** (Figure 3a,b) demonstrated not only expressed a chitosan peak (18–26° 2θ) but also intense peaks corresponding to $Cu(OAc)_2$ dihydrate (12.8°, 14.3°, 15,1°, 15,4°, 16.5° 2θ). These peaks indicate the preservation of copper(II) acetate dihydrate as a crystalline phase in the samples caused by the incomplete coordination of Cu^{2+} ions with chitosan. $Cu(OAc)_2$ dihydrate peaks were observed even when $CuSO_4$ was used as the source of Cu^{2+}, while no $CuSO_4$ peaks were observed. This is because a 1% acetic acid solution of chitosan was used to obtain the samples. Thus, the large excess of acetate ions in the solution, as well as the lower solubility of $Cu(OAc)_2$ dihydrate, in comparison with $CuSO_4$, resulted in the crystallization of Cu(II) in the acetate form ($Cu(OAc)_2$ dihydrate). It is also obvious that diffraction patterns of **7**–**12** exhibited extra peaks associated with the introduction of sodium hyaluronate into the composites.

According to X-ray diffraction data, samples **13**–**14** contain no $Cu(OAc)_2$ dihydrate phase, but rather contain $CuSO_4$ pentahydrate. Sample **15** revealed only traces of $CuSO_4$ pentahydrate. This is explained by the fact that due to the poor solubility of the starting CH-Chol in 1% acetic acid, a prolonged stirring of the reaction mixture (overnight) was required to achieve the conversion. Apparently, the dominant part of acetic acid could evaporate from the open beaker during this period of time. In the case of samples **16**–**18**, their X-ray diffraction patterns displayed $Cu(OAc)_2$ dihydrate peaks, and this is completely understandable, since we used copper(II) acetate to prepare **16**–**18**. In general, **13**–**18** contain higher fractions of the crystalline phase than **1**–**12**. This is due to the lower hydrophilicity and coordinating ability of the cholesterol–chitosan derivative used to obtain **13**–**18** compared to conventional chitosan involved in the preparation of **1**–**12**.

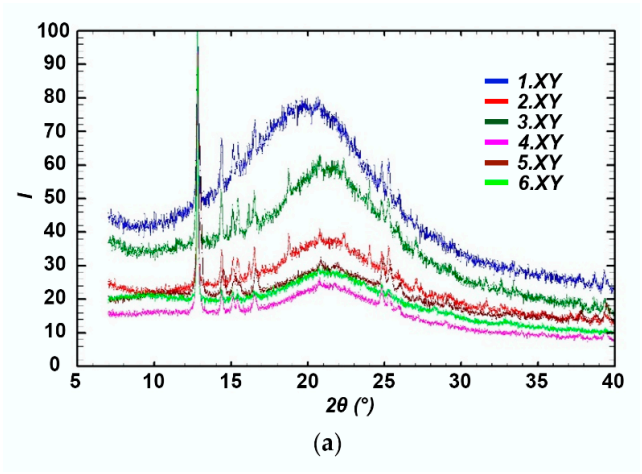

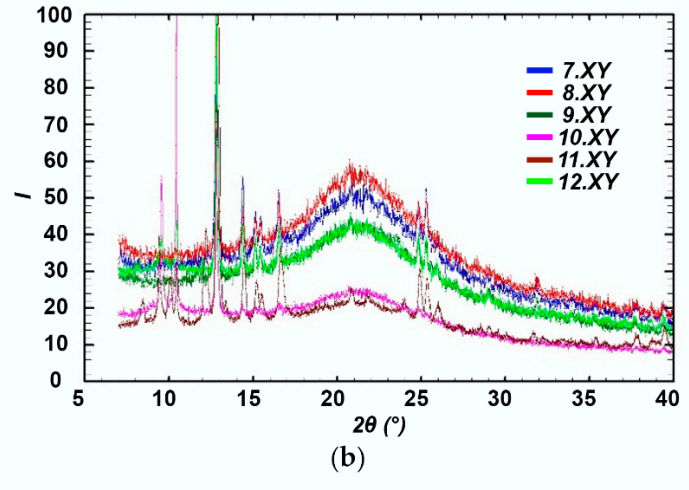

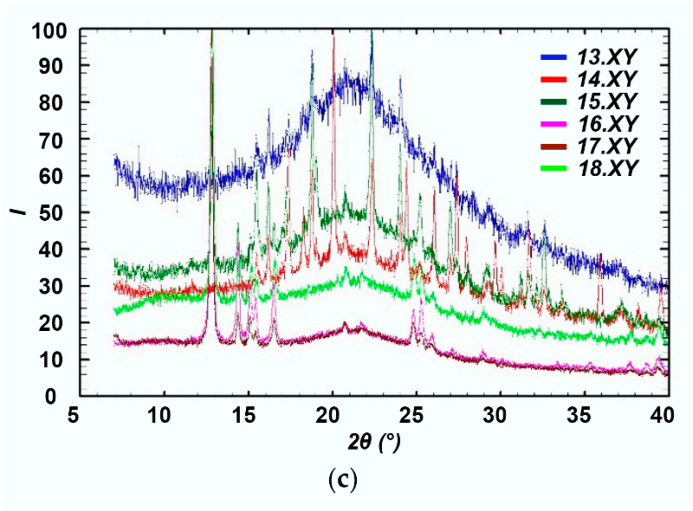

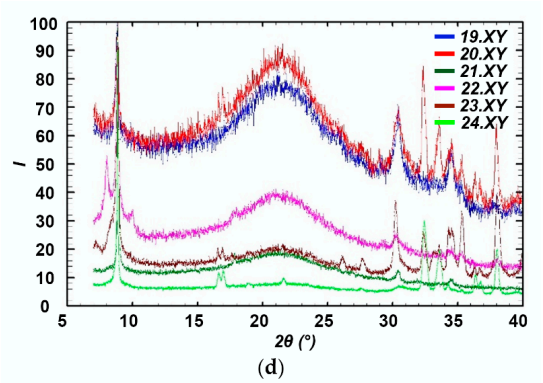

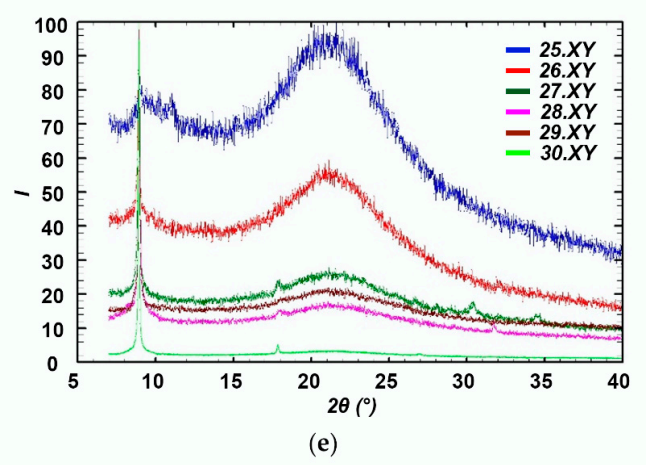

Figure 3. X-ray diffraction patterns of **1–6** (**a**), **7–12** (**b**), **13–18** (**c**), **19–24** (**d**), and **25–30** (**e**), normalized to the main peak intensity.

As for the succinated species **25–30**, their diffraction patterns are quite remarkable. These diffraction patterns are characterized by the absence of sets of crystalline peaks, which were observed for all previous samples **1–24**. Neither $Cu(OAc)_2$ dihydrate nor $CuSO_4$ were present in **25–30**. Therefore, Cu^{2+} ions are exclusively coordinated to the polymer. Additionally, X-ray diffraction data indicated a higher fraction of the amorphous phase therein.

Thus, the X-ray diffraction study showed that **1**–**24** contain (*i*) a polymer phase and (*ii*) crystalline copper(II) salt, while **25**–**30** contain mainly the polymer phase. The polymer phase is represented by chitosan (**1**–**12** and **19**–**30**) or its cholesterol derivative (**13**–**18**), as well as sodium hyaluronate (**1**–**12**, **25**–**30**). In addition, as mentioned above in Section 2.1.2, the polymer phase can exist both in the form of a coarse-grained powder (**4**–**6**, **10**–**12**, **16**–**18**, **22**–**24**) and in the form of nanoparticles (**1**–**3**, **7**– **9**, **13**–**15**, **19**–**21**, **25**–**30**).

It is important to note that samples **5** and **17** have similar and interesting characteristic features. Sample 17 is well crystallized and contains $Cu(OAc)_2$ dihydrate nanoparticles. Sample **5** also contains $Cu(OAc)_2$ dihydrate nanoparticles, as well as some unidentified impurities, as evidenced by a split peak at 12.8° 2θ.

The detected inorganic nanoparticles in samples **5** and **17** are described by the monoclinic syngony, space group A2/a. The calculated cell parameters were as follows: a = 13.840(1) Å, b = 8.564(4) Å, and c = 13.180(1) Å, β = 117.03(7)°. The maximum difference between the calculated and experimental positions of diffraction reflections did not exceed ~0.01°. To estimate the sizes of these $Cu(OAc)_2$ dihydrate nanoparticles, we approximated the X-ray diffraction profiles using the Pseudo-Voigt function and refined the peak position, intensity, and half-width. The refinement quality was controlled using statistical criteria. Crystallite sizes calculated using the Scherrer formula from the profiles of the first five peaks (maximum peak, reflection (0 1 1) and reflections (2 0 0), (0 0 2), (−2 0 2), and (−2 1 1)) were 315–486 Å (mainly ~380 Å, reflections (0 1 1), (2 0 0), and (−2 0 2)), and the average size was 387 Å.

FTIR

In addition to the IR spectra for all obtained samples, we also recorded the spectra of starting materials: chitosans (MW 12, 200, and 500 kDa), sodium hyaluronate, and copper(II) sulfate and acetate. The IR spectra of the starting materials are shown in Figures 4 and 5.

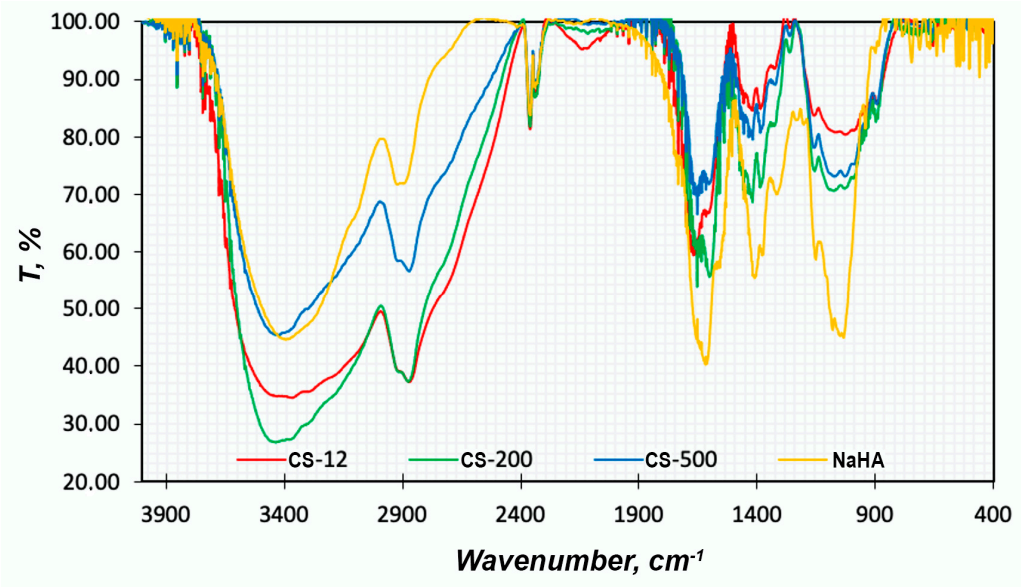

Figure 4. IR spectra of starting chitosans with different molecular weights and sodium hyaluronate.

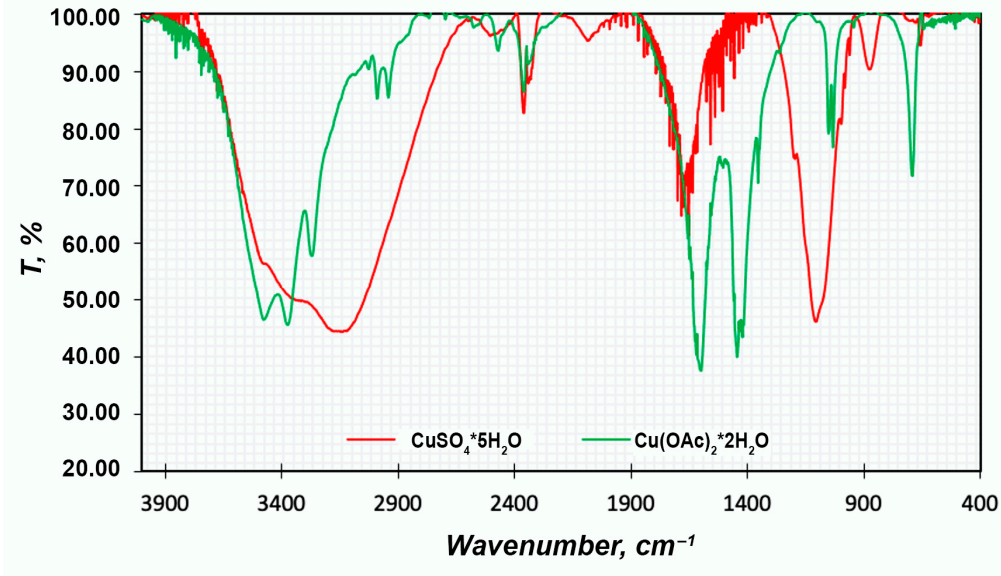

Figure 5. IR spectra of starting copper(II) salts.

The spectra of samples **1**–**6** (Figures 4 and 5) displayed a narrowing and weakening of a wide band at 3100–3500 cm^{-1}, corresponding to the stretching vibrations of O–H and N–H bonds. This narrowing of the band indicates a decrease in the involvement of the NH_2 and OH groups into hydrogen bonding caused by the coordination of the NH_2 and OH functionalities to the copper(II) center. Moreover, the band at 1653 cm^{-1} (bending vibrations of the NH_2 group) was shifted to 1604 cm^{-1}, which indicates the coordination of the amino groups of chitosan to the copper(II) center. The IR spectra **1**–**6** displayed (Figure 6) bands inherited from copper(II) acetate, which is consistent with the X-ray analysis data discussed above.

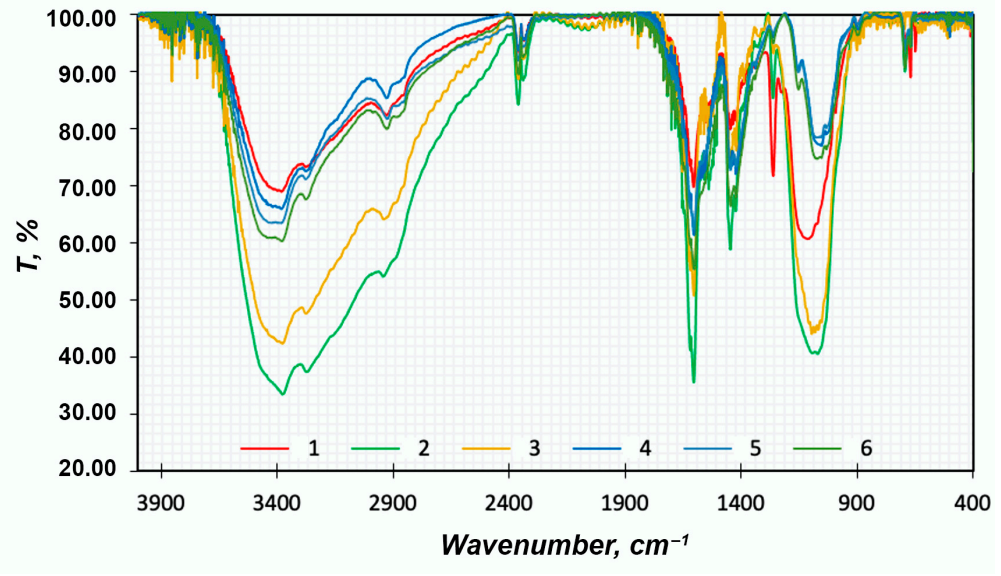

Figure 6. IR spectra of **1**–**6**.

The same trends were observed for the spectra of samples **7**–**12** (Figure 7).

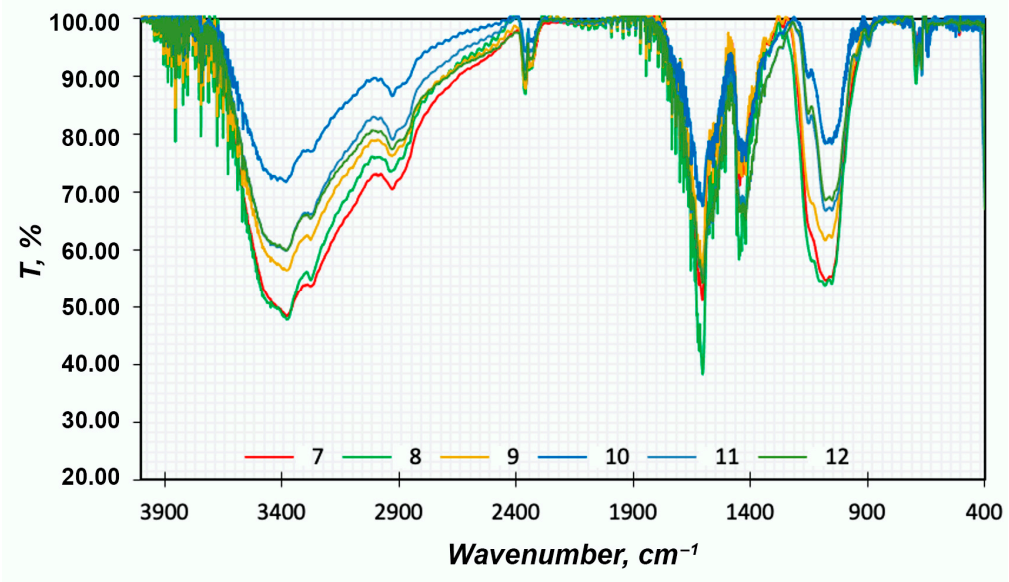

Figure 7. IR spectra of **7**–**12**.

The IR spectra of samples **13**–**18** (Figure 8) exhibited intense absorption bands, corresponding to the bands of the starting copper(II) salts. This is in agreement with the results of X-ray analysis indicating the presence of a large amount of the crystalline phase in the samples.

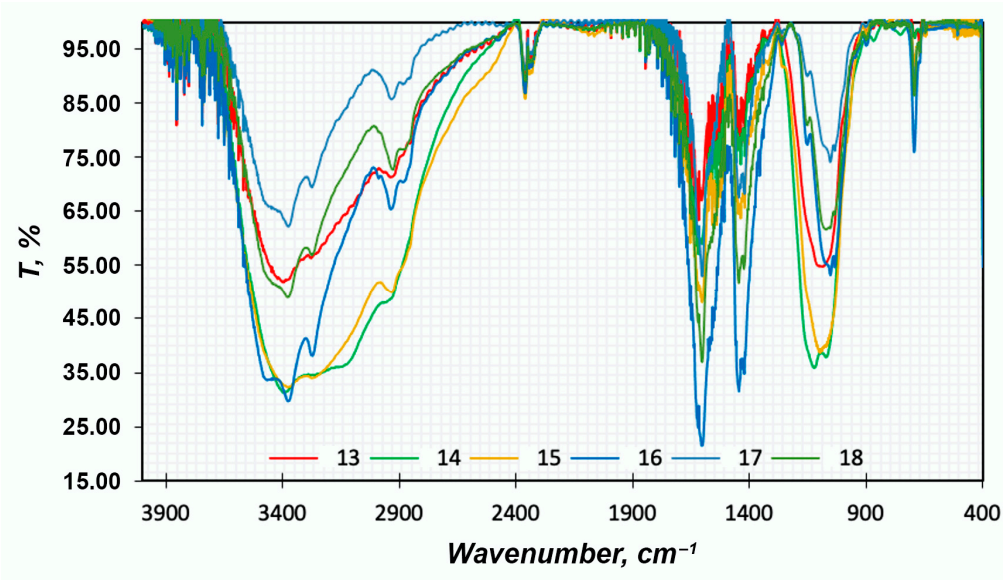

Figure 8. IR spectra of **13**–**18**.

The IR spectra of succinated samples **19**–**30** (Figures 9 and 10) showed a high-intensity band at 1630 cm^{-1}, which corresponds to the stretching vibrations of the C=O bond of the amide group. The amide bond arises as a result of succination (Scheme 2). An intense band at 1420 cm^{-1} was also observed, which corresponds to a deprotonated carboxylate group, which also confirms successful succination.

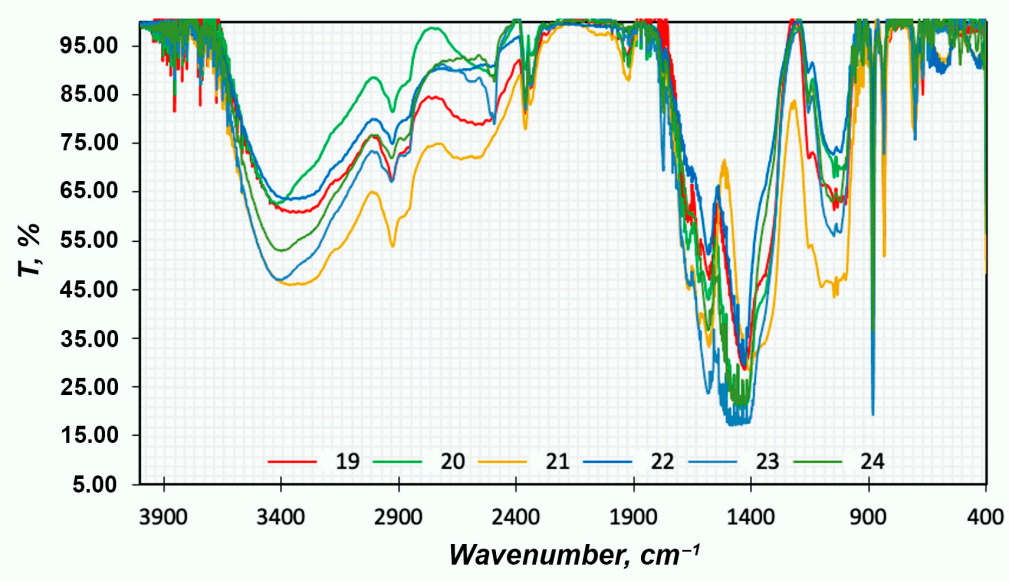

Figure 9. IR spectra of **19**–**24**.

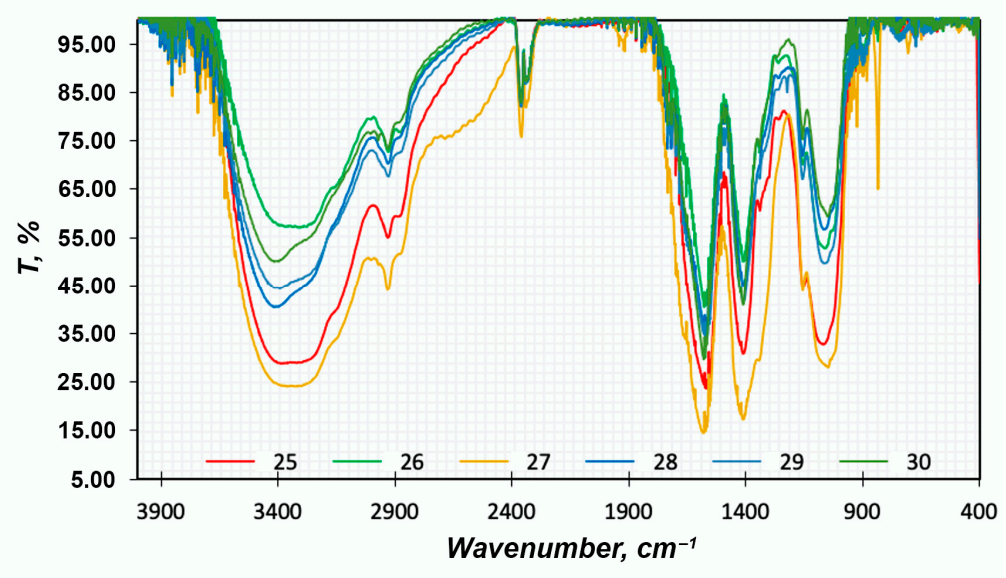

Figure 10. IR spectra of **25**–**30**.

TGA

To determine the thermal stability of the obtained systems, we carried out a thermogravimetric analysis for samples **21**–**25**, the results of which were used to determine the onset decomposition temperatures (the corresponding values are presented in Table 1).

According to Figure 11, the molecular weight of the starting chitosan did not significantly affect the thermal stability of the resulting composites. For similar samples, the onset decomposition temperatures were also close to each other. Only for samples obtained using copper(II) acetate were some differences in thermal stability observed, depending on the molecular weights of the chitosan.

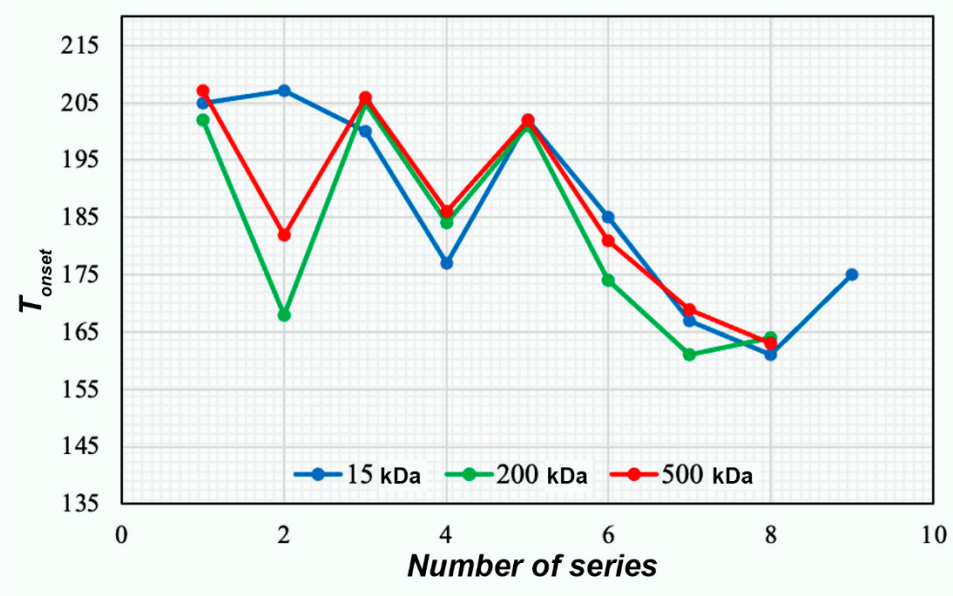

Figure 11. Dependence of the onset decomposition temperature on a series of samples for different molecular weights of chitosan.

Figure 12 plots the onset decomposition temperature versus number of series of samples, in which copper(II) sulfate or acetate was used as the source of copper(II) ions. As can be seen, the resultant samples were characterized by higher thermal stability when copper(II) sulfate was used.

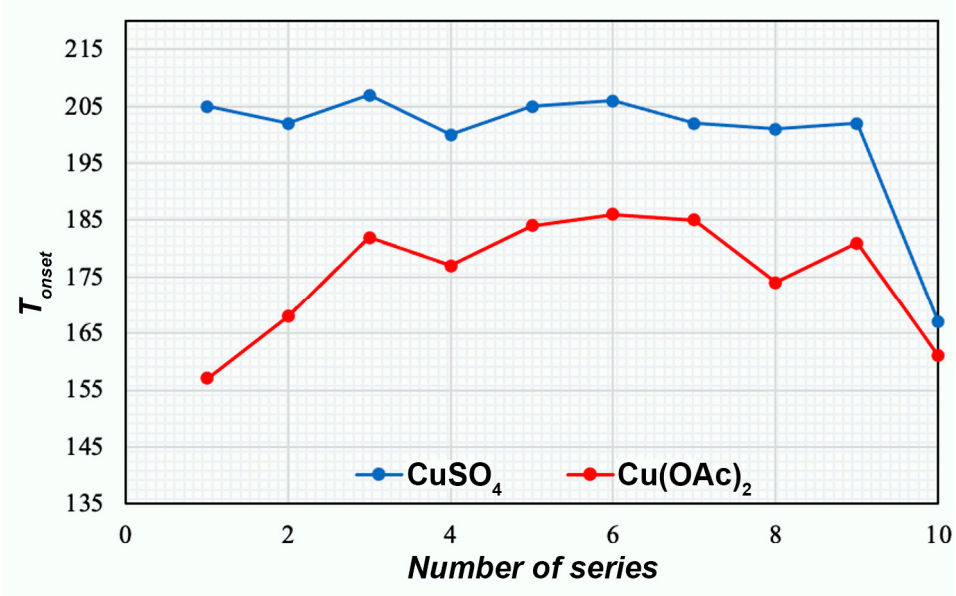

Figure 12. Dependence of onset decomposition temperature on a series of samples for different copper(II) salts.

Figure 13 displays dependences for the following different types of samples: CS + Cu(II) salt (**1**–**6**), CS + Cu(II) salt + NaHA (**7**–**12**), CS-Chol + Cu(II) salt (**13**–**18**), and CS + Cu(II) salt succinated (**19**–**24**). It can be seen that for the succinated samples, there was no dependence of the onset decomposition temperature on the type of Cu(II) salt used as a source of the Cu^{2+} ions.

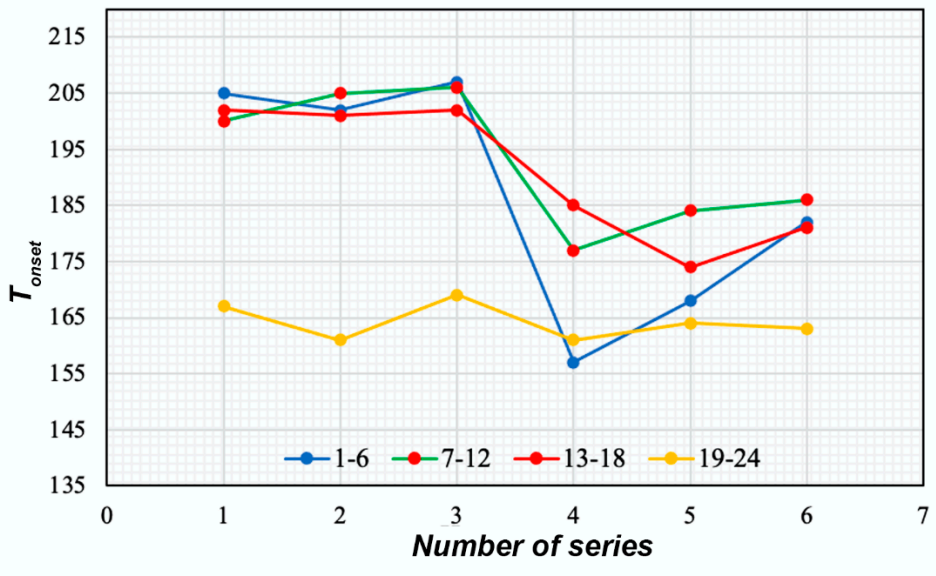

Figure 13. Dependence of onset decomposition temperature on a series of samples for different types of samples.

X-ray Fluorescence Analysis

The X-ray fluorescence analysis was designed to determine the elemental composition of the sample. Since the technique only detects the presence of elements heavier than sodium, we expected to detect only peaks corresponding to copper and, in the case of copper(II) sulfate content in the sample, peaks corresponding to sulfur.

We found no foreign elements in any of the recorded spectra. This fact is important for further studies of the catalytic activity of the composites, since even amounts of impurities of cations of other metals can determine the catalytic activity of materials [29]. Examples of the spectra are shown in Figures 14 and 15.

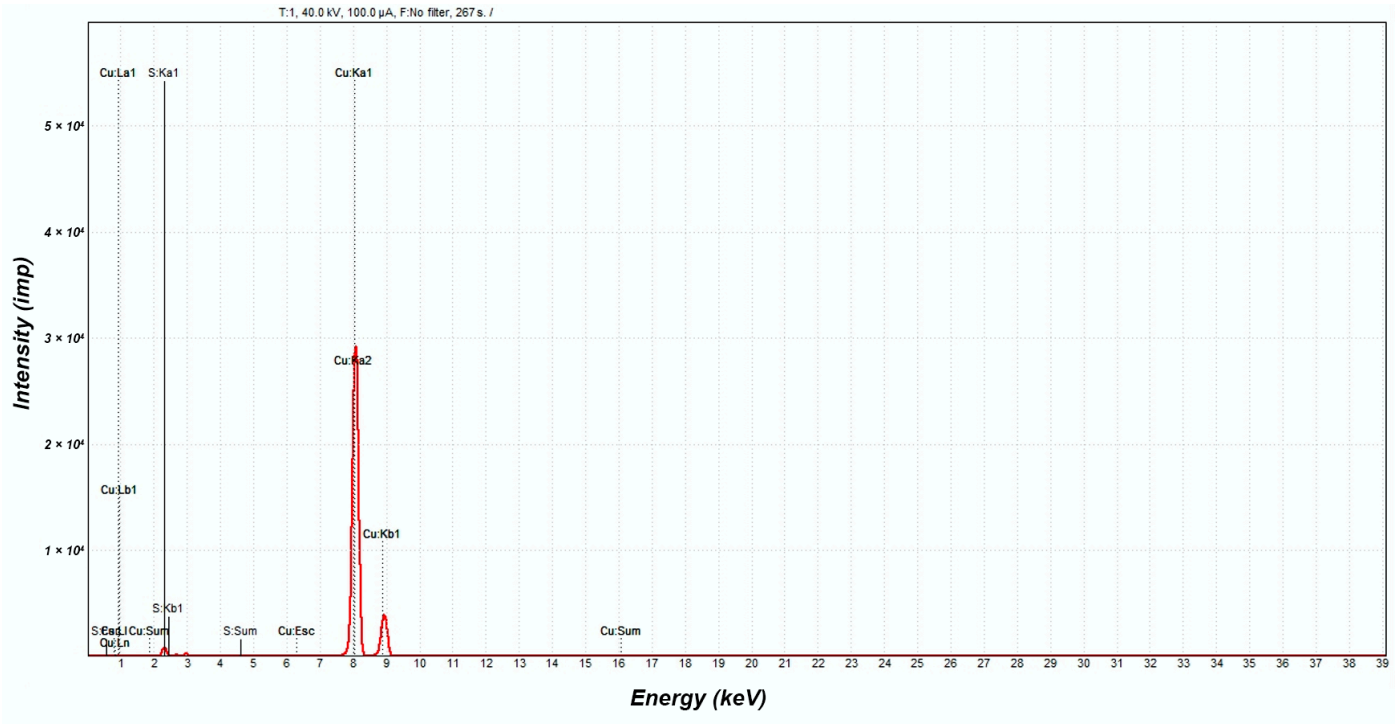

Figure 14. X-ray fluorescence spectrum of sample with copper(II) sulfate as a source of copper(II) ions.

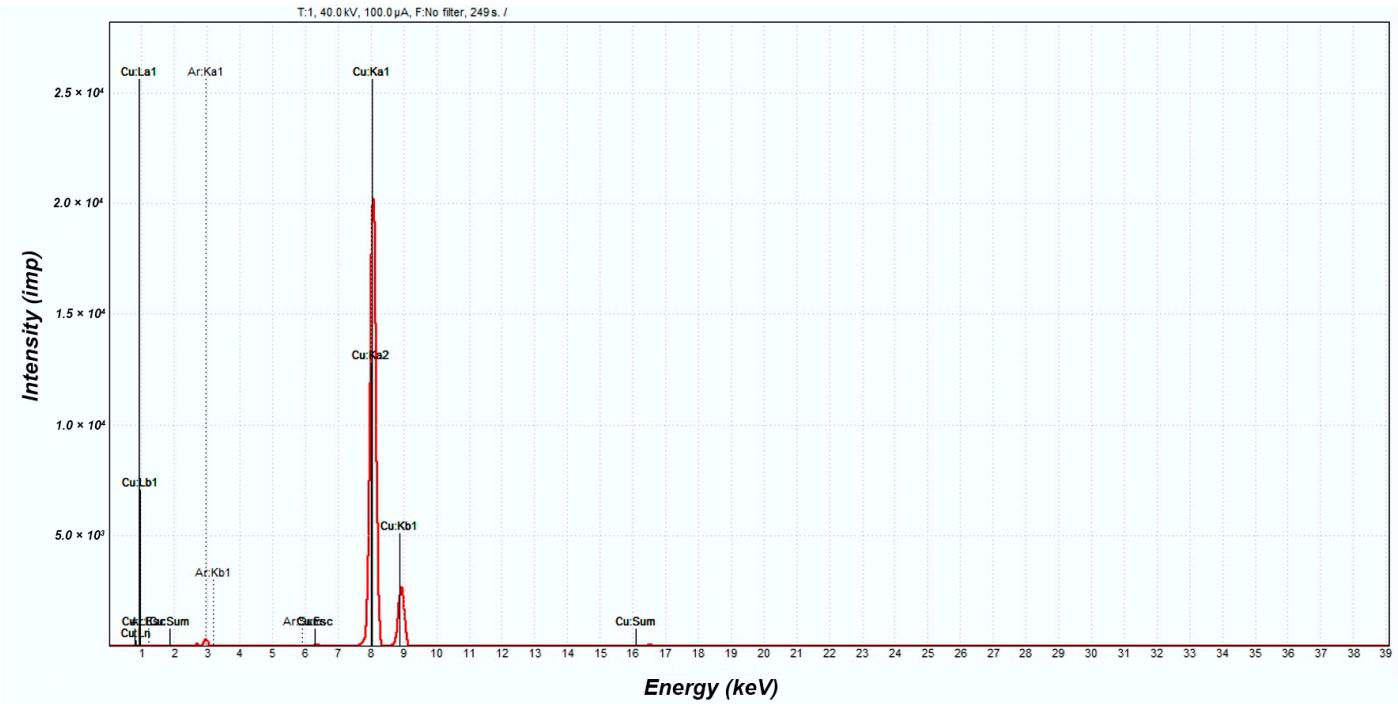

Figure 15. X-ray fluorescence spectrum of sample with copper(II) acetate as a source of copper(II) ions.

2.2. Catalytic Studies

2.2.1. Catalytic Studies of the Sonogashira Reaction

Since its discovery, the Sonogashira reaction (Scheme 3) remains among the most powerful C–C cross-couplings. The Sonogashira reaction is focused on the metal-catalyzed C–C bond formation between a terminal sp-hybridized carbon of an alkyne component and an sp^2-hybridized carbon atom of an aryl halide component. In many instances, a vinyl component can be involved into the Sonogashira cross-coupling instead of the aryl component. Moreover, aryl or vinyl halides can be replaced by the corresponding triflates.

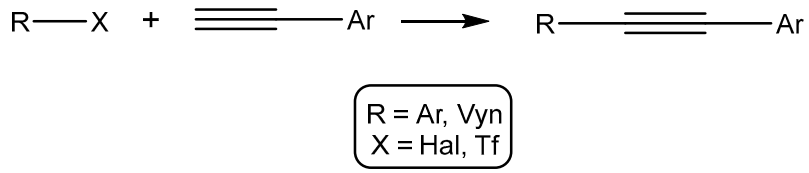

Scheme 3. The Sonogashira C–C cross-coupling reaction.

The Sonogashira reaction is widely employed in synthetic chemistry since it facilitates a wide array of challenging organic transformations as a part of the total synthesis of natural compounds, including plant or bacterial metabolites ((+)-(S)-laudanosine, (–)-(S)-xylopinine, and benzylisoquinoline or indole alkaloids), calicheamicin γ, dynemicin A, pyrrho-xanthin, callipeltoside A, and many other sophisticated natural metabolites, which are of paramount importance as bioactive compounds or starting materials in chemical biology studies. Recent outstanding advancements in this area are thoroughly reviewed in a recent paper [30]. The versatility of the Sonogashira reaction makes it an outstanding tool for the preparation of a range of pharmaceuticals. Thus, the Sonogashira reaction is used for the synthesis of sapinofuranone A [31]; (−)-harveynone [32], which possess antitumor activity [32]; (−)-tricholomenyn [32], which has antimitotic activity [33]; lappaconitine derivatives [34], exhibiting cardiotropic effects [35]; and many other important pharmacologically active compounds successfully employed in clinical practice (see review [36]).

A conventional protocol for the Sonogashira reaction implies a treatment of alkyne and aryl (or vinyl) components in toluene with a Pd-based catalyst in the presence of a Cu-based co-catalyst. Moreover, this complex catalytic system functions successfully only at high temperatures (above 100 °C) and under anaerobic conditions. Numerous efforts have been put forth for the development of new, highly efficient catalysts for the Sonogashira reaction, allowing the synthetic protocol to be adapted to milder and so-called "green" conditions.

The main trends in the development of new catalytic systems for the Sonogashira reaction emerging in the contemporary literature can be divided into three basic categories: (i) simplification of catalytic systems while making them capable of functioning under aerobic conditions; (ii) development of catalytic systems based on metals cheaper than palladium; (iii) the introduction of non-toxic, biocompatible, and biodegradable metals/ligands/supports in catalytic systems, as well as the use of eco-friendly solvents (as an essential part of the green chemistry concept) [37–39]. The ideal candidate, of course, must meet all three trends, but such examples are extremely rare in the literature.

In the current study, we evaluated the catalytic activity of the prepared samples **1–30,** which seem compliant with all three trends mentioned above. Firstly, **1–30** are simple systems, and their preparation procedure is extremely facile. Moreover, we conducted preliminary experiments and revealed that some of the **1–30** composites are capable of catalyzing the Sonogashira reaction under aerobic conditions. Secondly, copper, indeed, is sufficiently cheaper than palladium (ca. 8000 times). Thirdly, the elaborated catalytic systems **1–30** contain the chitosan macromolecule as ligand and support. Chitosan, in turn, is a naturally occurring carbohydrate polymer, which is biocompatible, biodegradable, and essentially non-toxic.

We performed catalytic tests for **1–30** in a model Sonogashira reaction under aerobic conditions in water. The model Sonogashira reaction is presented in Scheme 4.

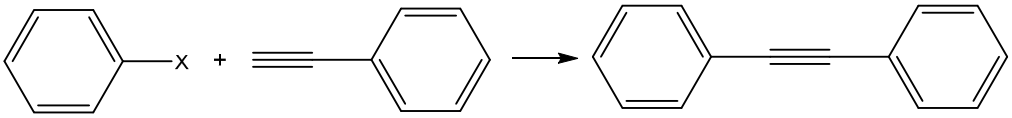

Scheme 4. The model Sonogashira reaction (X = Cl, Br, I).

For preliminary experiments, we used the following conditions: 20 mol% of catalyst, based on Cu^{2+}; an alkyne:aryl halide molar ratio of 1:1.1; K_3PO_4 as a base; boiling water; and a reaction time of 10 h. We found that only **13–18** demonstrated catalytic activity in the model Sonogashira reaction (Scheme 4, X = I, Table 2, entries **1–6**). Thus, samples **13–18** were chosen for further optimization of the catalytic conditions.

Table 2. Catalytic test results for the model Sonogashira reaction.

Entry	Catalyst	Base/X	mol%	T, °C	Time, h	Yield,%
1	**13**	K_3PO_4/I	20	100	10	54
2	**14**	K_3PO_4/I	20	100	10	56
3	**15**	K_3PO_4/I	20	100	10	50
4	**16**	K_3PO_4/I	20	100	10	18
5	**17**	K_3PO_4/I	20	100	10	16
6	**18**	K_3PO_4/I	20	100	10	16
7	**13**	K_2CO_3/I	20	100	10	58
8	**14**	K_2CO_3/I	20	100	10	60
9	**15**	K_2CO_3/I	20	100	10	60
10	**16**	K_2CO_3/I	20	100	10	22
11	**17**	K_2CO_3/I	20	100	10	22
12	**18**	K_2CO_3/I	20	100	10	20
13	**13**	Cs_2CO_3/I	20	100	10	59

Table 2. *Cont.*

Entry	Catalyst	Base/X	mol%	T, °C	Time, h	Yield,%
14	**14**	Cs_2CO_3/I	20	100	10	57
15	**15**	Cs_2CO_3/I	20	100	10	57
16	**16**	Cs_2CO_3/I	20	100	10	20
17	**17**	Cs_2CO_3/I	20	100	10	20
18	**18**	Cs_2CO_3/I	20	100	10	23
19	**13**	KF/I	20	100	10	40
20	**14**	KF/I	20	100	10	44
21	**15**	KF/I	20	100	10	45
22	**16**	KF/I	20	100	10	17
23	**17**	KF/I	20	100	10	17
24	**18**	KF/I	20	100	10	15
25–30	**13–18**	Et_3N or Py/I	20	100	10	traces
31	**13**	LiOH/I	20	100	10	100
32	**14**	LiOH/I	20	100	10	100
33	**15**	LiOH/I	20	100	10	100
34	**16**	LiOH/I	20	100	10	54
35	**17**	LiOH/I	20	100	10	53
36	**18**	LiOH/I	20	100	10	53
37	**13**	LiOH/I	20	90	3	100
38	**14**	LiOH/I	20	90	3	100
39	**15**	LiOH/I	20	90	3	100
40	**16**	LiOH/I	20	90	3	50
41	**17**	LiOH/I	20	90	3	52
42	**18**	LiOH/I	20	90	3	54
43	**13**	LiOH/Br	20	90	3	66
44	**14**	LiOH/Br	20	90	3	64
45	**15**	LiOH/Br	20	90	3	69
46	**13**	LiOH/Cl	20	90	3	31
47	**14**	LiOH/Cl	20	90	3	30
48	**15**	LiOH/Cl	20	90	3	26

Recent reviews and books have repeatedly emphasized that the base plays a very important role in this reaction. Thus, the choice of a suitable base is a key step in optimizing the reaction conditions, and this issue must be addressed for each catalytic system individually. During the course of evaluation of the effect of the base on the model reaction (Scheme 4, X = I), we identified lithium hydroxide to be most efficient (Table 2, entries **31**–**36**). Other tested bases (i.e., potassium carbonate, cesium carbonate, sodium orthophosphate, sodium fluoride) showed significantly weaker effects (Table 2, entries **1**–**24**). Organic bases, such as triethylamine and pyridine, were found to be inactive (Table 2, entries **25**–**30**).

Variations of reaction time and temperature demonstrated that the optimum temperature was 90 °C, and the optimum reaction time was 3 h (Table 2, entries **37**–**42**). A further decrease in temperature to 80 °C resulted in a decrease in the reaction yield. When the temperature was increased higher than 110 °C, the reaction lost its selectivity and furnished a broad mixture of compounds in addition to the desired cross-coupling product (6 spots in TLC). In this mixture, we identified, in particular, diyne Ph–C≡C–C≡C–Ph and the product of undesired oxidative homocoupling of the terminal acetylene Ph–C≡CH.

We also found that under all the aforementioned conditions, composites **16**–**18** (based on copper(II) acetate and occurring in the form of coarse-grained powder) demonstrated much lower catalytic activity than **13**–**15** (based on copper(II) sulfate and occurring as nanoparticles). Thus, nanoparticles **13**–**15** were the most promising catalytic systems for the Sonogashira reaction under aerobic conditions in water (Table 2, entries **1**–**42**).

All the above-listed results were valid for the model Sonogashira reaction (Scheme 4) when X = I. In contrast, the yields of the cross-coupling product were much lower when the aryl bromide (X = Br) and aryl chloride (X = Cl) were involved in the model reaction as the aryl components (Table 2, entries **43**–**48**).

Figure S1 shows the ^{1}H NMR spectrum of the Sonogashira reaction product.

2.2.2. Catalytic Studies of the Buchwald–Hartwig and Chan–Lam Reactions

The Buchwald–Hartwig and Chan–Lam reactions are similar reactions represented by the palladium-catalyzed C–N cross-couplings between aryl halogenide (Buchwald–Hartwig reaction) or aryl boronic acid (Chan–Lam reaction) and primary or secondary amines [40,41] (Scheme 5). The C–N cross-couplings are an essential tool for the synthesis, especially in preparative chemistry, of biologically active substances and pharmaceuticals. A classic synthetic protocol for the Buchwald–Hartwig and Chan–Lam reactions implies the use of sufficiently hazardous solvents under anaerobic conditions. Improvements to these protocols include the development of cheap metal-based and simple ligand-based catalyst systems that can operate under aerobic conditions in eco-friendly solvents [40,41].

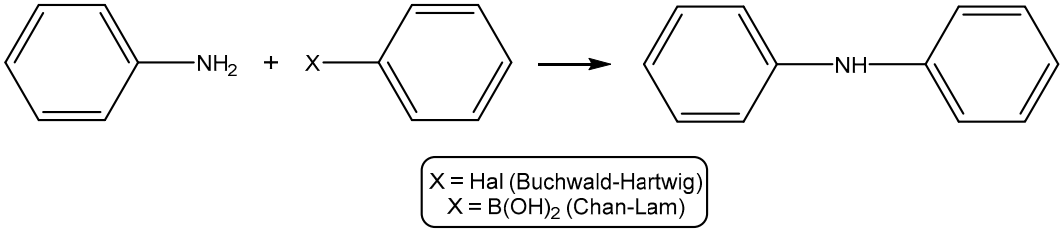

Scheme 5. The model Buchwald–Hartwig and Chan–Lam C–N cross-coupling reactions.

Herein, we tested the catalytic activity of **1**–**30** in the model Buchwald–Hartwig and Chan–Lam C–N cross-couplings (Scheme 5). For condition optimization, we also used 20 mol% (based on Cu^{2+}) of catalysts **1**–**30**. At the preliminary stages of our work, we found that only **13**–**18** were able to catalyze the model reactions. The results are presented in Table 3. However, preliminary experiments demonstrated low yields of both cross-couplings in water even under harsh anaerobic conditions, i.e., 120 °C, 24 h (Table 3, entries **1**–**12**). This was not surprising, as the literature is abundant with such reports [42]. Conventionally, to overcome this obstacle, I^--containing additives (KI, ZnI_2, etc.) are used [43,44]. By applying this approach, we were able to achieve high yields of desired products in the model reactions (Scheme 5, X = I, Table 3, entries **13**–**24**)) even under aerobic conditions. The best catalytic results were demonstrated by **13**–**15**; therefore, they were used for further experiments (Table 3, entries **13**–**15** and **19**–**21**).

Table 3. Catalytic studies of the model Buchwald–Hartwig and Chan–Lam C–N cross-coupling reactions.

Entry	Catalyst	X	mol%	T (°C)	Time (h)	Yield (%)
1 *	**13**	I	20	120	24	18
2 *	**14**	I	20	120	24	15
3 *	**15**	I	20	120	24	16
4 *	**16**	I	20	120	24	traces
5 *	**17**	I	20	120	24	traces
6 *	**18**	I	20	120	24	traces
7 *	**13**	$B(OH)_2$	20	120	24	23
8 *	**14**	$B(OH)_2$	20	120	24	22
9 *	**15**	$B(OH)_2$	20	120	24	20
10 *	**16**	$B(OH)_2$	20	120	24	5
11 *	**17**	$B(OH)_2$	20	120	24	5
12 *	**18**	$B(OH)_2$	20	120	24	5
13	**13** + ZnI_2	I	20	120	24	100
14	**14** + ZnI_2	I	20	120	24	100

Table 3. *Cont.*

Entry	Catalyst	X	mol%	T (°C)	Time (h)	Yield (%)
15	**15** + ZnI_2	I	20	120	24	100
16	**16** + ZnI_2	I	20	120	24	43
17	**17** + ZnI_2	I	20	120	24	40
18	**18** + ZnI_2	I	20	120	24	40
19	**13** + ZnI_2	$B(OH)_2$	20	120	24	100
20	**14** + ZnI_2	$B(OH)_2$	20	120	24	100
21	**15** + ZnI_2	$B(OH)_2$	20	120	24	100
22	**16** + ZnI_2	$B(OH)_2$	20	120	24	48
23	**17** + ZnI_2	$B(OH)_2$	20	120	24	50
24	**18** + ZnI_2	$B(OH)_2$	20	120	24	45
25	**13** + ZnI_2	I	20	120	15	100
26	**14** + ZnI_2	I	20	120	15	100
27	**15** + ZnI_2	I	20	120	15	100
28	**13** + ZnI_2	$B(OH)_2$	20	120	15	100
19	**14** + ZnI_2	$B(OH)_2$	20	120	15	100
30	**15** + ZnI_2	$B(OH)_2$	20	120	15	100
31	**13** + ZnI_2	I	20	100	15	51
32	**14** + ZnI_2	I	20	100	15	54
33	**15** + ZnI_2	I	20	100	15	48
34	**13** + ZnI_2	$B(OH)_2$	20	100	15	55
35	**14** + ZnI_2	$B(OH)_2$	20	100	15	55
36	**15** + ZnI_2	$B(OH)_2$	20	100	15	59
37	**13** + ZnI_2	I	20	80	15	0
38	**14** + ZnI_2	I	20	80	15	0
39	**15** + ZnI_2	I	20	80	15	0
40	**13** + ZnI_2	$B(OH)_2$	20	80	15	traces
41	**14** + ZnI_2	$B(OH)_2$	20	80	15	traces
42	**15** + ZnI_2	$B(OH)_2$	20	80	15	traces
43	**13** + ZnI_2	Br	20	120	15	100

* anaerobic conditions.

In the next step, we estimated the optimum reaction time and temperature. At a temperature of 120 °C, the optimum time for both reactions was 15 h (Table 3, entries **25**–**30**). If the reactions run for 14 h, this already results in a decrease in the effective yields. Reducing the temperature is disadvantageous for these reactions, since it leads to a sharp decrease in the yields (100 °C, Table 3, entries **31**–**36**) or even termination of the reactions (80 °C, Table 3, entries **37**–**42**).

For the model Buchwald–Hartwig cross-coupling, we found that the type of halogen atom is also important. Thus, if X = I or Br, the reaction yield is ca. 100% (Table 3, entries **43**–**45**). In contrast, the reaction yield decreases dramatically to ca. 60% on going from aryl iodides and bromides to chlorides (Table 3, entries **37**–**42**).

Figure S2 shows the ^{1}H NMR spectrum of the Buchwald–Hartwig and Chan–Lam reactions product.

2.2.3. Catalytic Studies of the Aldol Reaction

The aldol reaction is also among most powerful tools for the C–C bond formation in synthetic chemistry, and it has not lost its actuality since its discovery in the 19th century [45]. The aldol reaction is a sort of coupling between two aldehyde or ketone molecules, where one of the molecules plays the role of a nucleophile, and the second acts as an electrophile (Scheme 6).

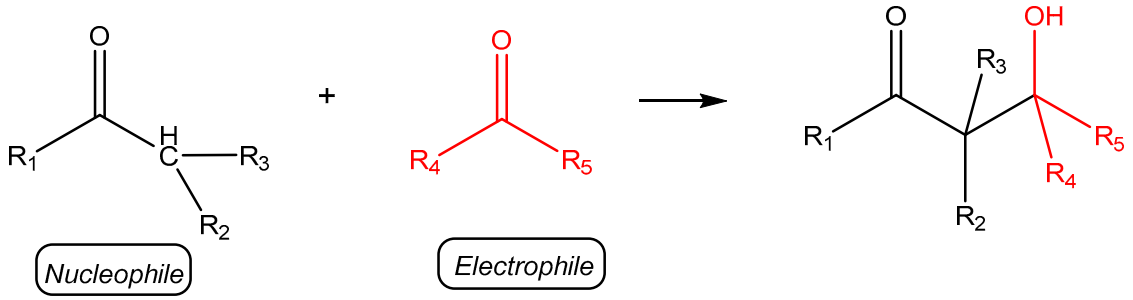

Scheme 6. The aldol reaction.

Many important natural compounds contain structural blocks, or synthons, corresponding to components of the aldol reaction [46,47]. The industrial synthesis of pentaerythritol (the starting compound to produce many formulations) [48], as well as the industrial production of atorvastatin (a cholesterol-lowering drug), is based on the aldol reaction [49,50]. Immunomodulatory compounds (e.g., FK506), antifungal drugs (e.g., amphotericin B), and even anti-cancer bioactives (e.g., discodermolide) can also be synthesized using the aldol reaction [51].

The main disadvantages of traditional aldol reaction protocols are the use of harsh alkaline catalysts (sodium ethoxide, sodium diisopropylamide), the use of non-aqueous solvents, and frequent undesired side reactions (conversion of the forming aldol into the corresponding olefine). In addition, often a strong base is used not in a catalytic, but in a stoichiometric amount [45]. These limitations, as well as the challenges of green chemistry, have spurred the development of new, highly efficient aldol catalysts, and these studies are relevant and up to date (see reviews [52,53]).

In this study, we tested Cu(II)/chitosan composites **1**–**30** in the model aldol reaction between acetone (as a nucleophilic component) and 4-nitrobenzaldehyde (as an electrophilic component) (Scheme 7).

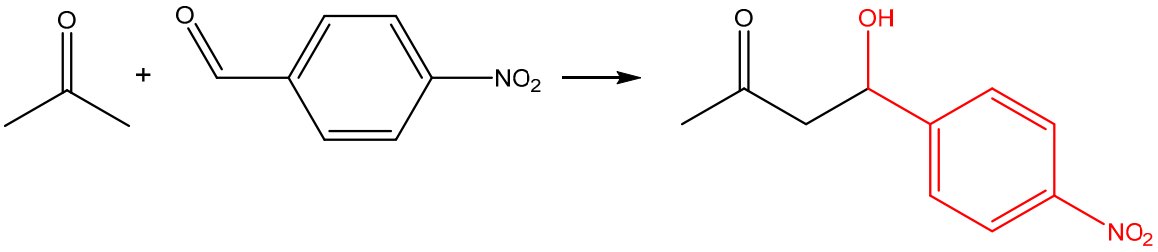

Scheme 7. The model aldol reaction.

As a result of preliminary experiments in water at 50 °C (3 h), we found that the most efficient catalysis of the aldol reaction was achieved using catalytic systems **25**–**30** (Table 4, entries **1**, **6**, **11**, **16**, **21**, **26**). All other systems proved to be inactive—their use caused at best the appearance of only traces of the desired product. Thus, **25**–**30** was selected for further studies. By varying the reaction conditions (Table 4), we demonstrated that the optimum temperature was at ca. 60 °C, and the optimum reaction time was 4 h. Applying these conditions (with a molar ratio of acetone:aldehyde of 3:1 and 20 mol% of the catalyst), we achieved almost quantitative yields of the product (Table 4, entries **3**, **8**, **13**, **18**, **23**, **28**). Figure S3 shows the ^{1}H NMR spectrum of the aldol reaction product.

Table 4. Catalytic studies of the model aldol reaction.

Entry	Catalyst	mol%	T (°C)	Time (h)	Yield (%)
1	**25**	20	50	3	42
2	**25**	20	60	3	90
3	**25**	20	60	4	100
4	**25**	10	60	4	80
5	**25**	50	60	3	90
6	**26**	20	50	3	40
7	**26**	20	60	3	90
8	**26**	20	60	4	100
9	**26**	10	60	4	83
10	**26**	50	60	3	90
11	**27**	20	50	3	44
12	**27**	20	60	3	92
13	**27**	20	60	4	100
14	**27**	10	60	4	78
15	**27**	50	60	3	90
16	**28**	20	50	3	40
17	**28**	20	60	3	90
18	**28**	20	60	4	100
19	**28**	10	60	4	83
20	**28**	50	60	3	90
21	**29**	20	50	3	37
22	**29**	20	60	3	90
23	**29**	20	60	4	100
24	**29**	10	60	4	80
25	**29**	50	60	3	92
26	**30**	20	50	3	43
27	**30**	20	60	3	92
28	**30**	20	60	4	100
29	**30**	10	60	4	85
30	**30**	50	60	3	93

2.2.4. Catalytic Studies of the 1,3-Dipolar Cycloaddition of Nitrile Oxides to Nitriles

The 1,3-dipolar cycloaddition ([3+2]-cycloaddition) between a dipole and a dipolarophile is the most powerful one-stage way for the construction of five-membered heterocycles, including those of biomedical importance [54]. Nitrile oxides belong to the so-called propargyl anion type of dipoles, and they are isoelectronic to organic azides. For organic azides, the 1,3-dipolar addition reactions are widely known, even for such inert dipolarophiles as nitriles (they were discovered in 2011 by two-time Nobel laureate Barry Sharpless) [55]. The cycloaddition of organic azides to nitriles is efficiently catalyzed by Zn^{2+} ions and many other suitable metal centers [56]. In contrast to azides, no metal-catalyzed cycloadditions of nitrile oxides to nitrile functionality have been described. The rare examples that can be found in the literature focused on the cycloaddition of nitrile oxides to nitrile ligands in their kinetically inert platinum or palladium complexes [57]. However, in this case, the reaction is not formally catalytic, since the resulting heterocycle remains in the coordination sphere of the complex; i.e., the catalytic cycle is not closed.

We were intrigued by the following question: Are **1**–**30** capable of catalyzing the 1,3-dipolar cycloaddition of nitrile oxides to nitriles? Preliminary experiments have shown that traditional nitriles containing electron-donating alkyl substituents (MeCN, EtCN) or weakly electron-withdrawing substituents (PhCN) interact with nitrile oxides neither in water nor in the corresponding nitrile medium, even under harsh conditions (120 °C, 24 h). There was no point in studying the catalytic activity of **1**–**30** in the reaction of nitrile oxides with nitriles containing strong electron acceptors (CCl_3CN), since these reactions proceed spontaneously on heating without any catalyst [58].

However, the literature describes a special type of nitriles, the so-called push–pull nitriles, which are often superior in their reactivity to traditional nitriles (alkyl- and aryl-

nitriles). Push–pull nitriles include dialkylcyanamides Alk_2NCN [59]. To the best of our knowledge, there are no reports on the metal-free or metal-catalyzed cycloaddition of nitrile oxides to push–pull nitriles. However, we were surprised that some of the composites **1–30** were able to catalyze the model reaction of cycloaddition of nitrile oxides to push–pull dimethylcyanamide nitrile (Scheme 8).

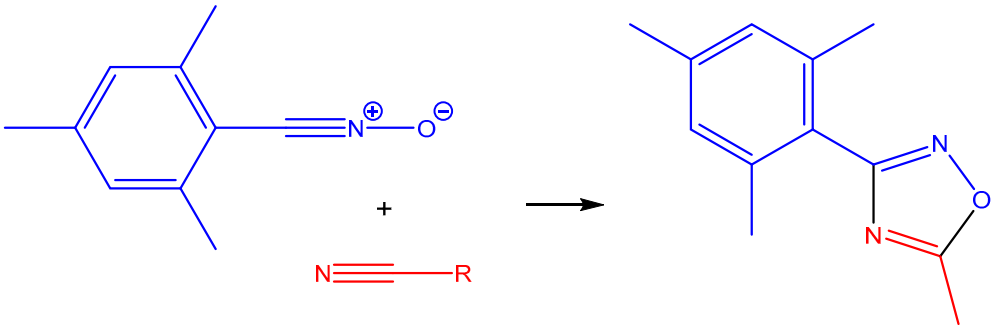

Scheme 8. The model 1,3-dipolar cycloaddition reaction.

We found that among **1–30,** only **5** and **17** catalyzed the model reaction (in the dimethylcyanamide medium). The TLC monitoring showed that the reaction proceeded at 80 °C, giving rise to the selective formation of the desired heterocycle. The composite **17** was proven to be most efficient (the reaction time for **17** was 3 h, while for **5**, the reaction time was 12 h or more). An increase in temperature led to a loss of selectivity of the reaction (5 spots on TLC).

Thus, **17** efficiently catalyzes the cycloaddition of nitrile oxides to dialkylcyanamides. Of course, expanding the range of push–pull nitriles and nitrile oxides with various substituents is very interesting in order to broaden the limits of the discovered catalysis, and this project is underway in our group.

Figure S4 shows the ^1H NMR spectrum of the product of the 1,3-dipolar cycloaddition of nitrile oxides to nitriles.

2.2.5. Final Remarks on Catalytic Studies

The results of the catalytic studies should be considered from the following perspectives.

Firstly, we revealed that **13–15** are efficient aerobic catalysts for the studied three cross-couplings (Sonogashira, Buchwald–Hartwig, and Chan–Lam reactions) in water. The studied *C,N* cross-couplings (Buchwald–Hartwig and Chan–Lam reactions) catalyzed by **13–15** require ZnI_2 for successful catalysis, while the studied *C,C* cross-coupling (Sonogashira reaction) requires only the presence of a strong base, i.e., LiOH. This indicates that copper(II) is the catalytic species in the Sonogashira reaction, while copper(I) is the catalytic species in the Buchwald–Hartwig and Chan–Lam reactions. It is important that among all tested catalysts **1–30**, only **13–18** were capable of catalyzing the studied cross-couplings in water. This fact suggests that not only copper(I or II) is necessary for successful catalysis, but also the cholesterol moiety in the composition of the catalytic system. We believe that the cholesterol moiety, due to its hydrophobic binding to cross-coupling substrates, ensures their efficient interaction with the metal center. Among catalysts **13–18**, **13–15** turned out to be the most efficient, and this is not surprising, because they are dispersed to the nano level. An increase in the catalytic activity of chitosan-based systems upon going to sizes smaller than 1000 nm is a classic issue in modern catalysis science and has been repeatedly described in recent reviews [60,61].

Secondly, we found that **25–30** were the most active catalysts for the aldol reaction in water among all **1–30** tested systems. We suppose that this can be explained by the synergism of the catalytic capabilities of copper(II) ions, chitosan, and sodium hyaluronate, as well as by the small size of catalytic particles (about 600 nm).

Thirdly, we established that **5** and **17** are able to catalyze the 1,3-dipolar cycloaddition of nitrile oxides to push–pull nitriles, i.e., dialkylcyanamides. Interestingly, only the mentioned **5** and **17** composites contain nanoparticles of copper(II) acetate dihydrate. Obviously, it is the presence of nanoparticles that provides the efficient catalysis of the studied cycloaddition by **5** and **23**. The highest catalytic effect is characteristic for cholesterol-containing system **17**. We believe that this is the result of the functioning of the cholesterol moieties in catalytic systems (similarly as described above for cross-couplings).

Fourthly, we confirmed the recyclability of catalytic systems (**13**–**15** in the model cross-couplings, **25**–**30** in the model aldol reaction, and **17** in the model dipolar cycloaddition). The systems do not lose their catalytic activity even after ten runs.

Fifthly, we determined that all studied model reactions are catalyzed genuinely by the corresponding chitosan/copper(II)-based systems rather than by leached copper species (**13**–**15**, **25**–**30**, and **17**). For this purpose, we carried out the model reactions with the corresponding catalyst under optimum conditions (see Section 3) until the effective conversion approached 50%. After that, the reaction mixture was subjected to centrifugation followed by filtration to completely remove catalysts **13**–**15**, **25**–**30**, or **17**. Continued heating of the filtrate under optimum conditions (see Section 3) did not lead to a further increase in conversion. This observation is convincing proof of the catalysis of the studied reactions directly by **13**–**15**, **25**–**30**, or **17**.

Finally, we also conducted blank experiments for all studied catalytic reactions. The experiments consisted of processing the starting materials under the same conditions but in the absence of catalysts **13**–**15**, **25**–**30**, or **17**. In all cases, no formation of the desired product was detected, and only traces of the target product were observed in the case of the aldol reaction. This fact is convincing evidence that the reactions under study are catalyzed directly by **13**–**15**, **25**–**30**, or **17**.

3. Materials and Methods

3.1. Materials

Chitosan of viscosity-average molecular weights 12, 200, and 500 kDa and degree of acetylation 10% was purchased from Bioprogress (Moscow, Russia). Copper(II) sulfate pentahydrate, copper(II) acetate dehydrate, potassium phosphate, potassium and cesium carbonates, potassium fluoride, lithium hydroxide, and zinc iodide were from Sigma Aldrich. Succinic anhydride, triethylamine, pyridine, phenylacetylene, 4-methoxy chloro-(bromo- or iodo-) benzene, phenyl boronic acid, chloro- (bromo- or iodo-) benzene, acetone, 4-nitrobenzaldehyde, dimethylcyanamide, and nitrile oxide (2,4,6-trimethyl phenylcyanide *N*-oxide) were also from Sigma Aldrich (Burlington, NJ, USA). Other chemicals and solvents were also from commercial sources and used as received without any further purification.

3.2. Preparation and Characterization of Chitosan/Copper(II) Composites

1–**6**. Chitosan (0.150 g) was dissolved in 150 mL of 1% CH_3COOH and stirred for 1 h. $CuSO_4 \times 5H_2O$ or $Cu(CH_3COO)_2 \times 2H_2O$ (0.150 g) was dissolved in 150 mL of distilled water and stirred for 1 h. The resulting chitosan solution was transferred into a 1 L beaker and mixed very intensely with a mechanical stirrer. The copper(II) salt solution was poured as a thin stream to the vigorously stirred solution of chitosan, and the resulting mixture was intensely stirred for 5 min. As a result, a slightly cloudy blue mixture was obtained, which was frozen and freeze-dried.

7–**12**. Chitosan (0.150 g) was dissolved in 150 mL of 1% CH_3COOH and stirred for 1 h. $CuSO_4 \times 5H_2O$ or $Cu(CH_3COO)_2 \times 2H_2O$ (0.150 g) was dissolved in 150 mL of distilled water and stirred for 1 h. A sodium hyaluronate load (0.150 g) was dissolved in 150 mL of distilled water and stirred for 1 h. The resulting chitosan solution was transferred into a 1 L beaker and stirred intensely with a mechanical stirrer. The copper(II) salt solution was poured as a thin stream to the stirring solution of chitosan, and then the sodium hyaluronate solution was poured as a thin stream, and the resulting mixture was intensively mixed for 5 min. A cloudy, opalescent mixture was obtained, which was frozen and freeze-dried.

13–18. Chitosan–cholesterol conjugate [62] (degree of substitution 3%) was dissolved in 1% acetic acid to obtain a solution with a concentration of 1 mg/mL. $CuSO_4 \times 5H_2O$ or $Cu(CH_3COO)_2 \times 2H_2O$ was dissolved in water to give a 1 mg/mL solution. The resulting chitosan solution was transferred into a 1 L beaker and vigorously stirred with a mechanical stirrer. The Cu(II) salt solution was added as a thin stream to the stirring solution of chitosan–cholesterol conjugate. The resulting mixture was frozen and freeze-dried.

19–30. Ten milliliters of ethyl acetate and 0.300 g of succinic anhydride were added to 0.100 g of any of **19–30**, and the resulting mixture was vigorously stirred overnight at 40 °C. The reaction mixture was centrifuged, and the precipitate was washed with ethyl acetate, water, 5% sodium bicarbonate solution, and again water. The washed precipitate was dispersed in water (15 mL), and the resulting suspension was frozen and freeze-dried.

3.3. Catalytic Experiments

3.3.1. Sonogashira Reaction

Catalytic activity screening was performed according to the slightly modified procedure described by us previously [63]. Briefly, the reaction vial was loaded with aryl halide from Table 2 (100 mg, 1 equiv), base from Table 2 (2.5 equiv), phenylacetylene (1.5 equiv), the tested catalyst (20 mol% based on Cu), and water (15 mL) and equipped with a Teflon-coated magnetic stirrer bar. The vial was closed with a septum and aluminum crimp seal and kept in an oil bath (for temperature and time, see Table 2). After cooling to room temperature, the reaction mixture was evaporated to dryness, and 1,2-dimethoxyethane (1 equiv; used as an NMR internal standard) was added. The content of the vial was extracted with three portions of $CDCl_3$; all fractions were combined, dried over Na_2SO_4, and analyzed by ^{1}H NMR spectroscopy. The product peak assignments were based on the published data [64], while quantifications were performed via the integration of the selected peaks of the product and comparison of their intensities with those of the standard.

3.3.2. Buchwald–Hartwig and Chan–Lam Reactions

The reaction vial was loaded with aniline (100 mg, 1 equiv), aryl halide (see Table 3) or phenylboronic acid (1.7 equiv), the tested catalyst (20 mol% based on Cu), and water (15 mL) and equipped with a Teflon-coated magnetic stirrer bar. The vial was closed with a septum and aluminum crimp seal and kept in an oil bath (for temperature and time, see Table 3). After cooling to room temperature, the reaction mixture was evaporated to dryness, and 1,2-dimethoxyethane (1 equiv; used as an NMR internal standard) was added. The content of the vial was extracted with three portions of $CDCl_3$; all fractions were combined, dried over Na_2SO_4, and analyzed by ^{1}H NMR spectroscopy. The product peak assignments were based on the published data [65], while quantifications were performed via the integration of the selected peaks of the product and comparison of their intensities with those of the standard.

3.3.3. Aldol Reaction

The catalytic experiments on the aldol reaction were performed completely according to the standard procedure reported by some of us previously [66].

1,3-Dipolar Cycloaddition Reaction

Nitrile oxide (0.100 g, 1 equiv) was dissolved in dimethylcyanamide (0.5 mL), and the tested catalyst (**5**, **11**, **17**, or **23**; 20 mol% based on Cu) was added into the reaction flask. The reaction mixture was stirred at 80 °C for 3 h (**17**) or 12 h (**5**, **11**, or **23**). The reaction was monitored by TLC. After total conversion of nitrile oxide (TLC monitoring), the solvent was evaporated in vacuo, and tetraethyl orthosilicate (1 equiv; used as an NMR internal standard) was added. The content of the flask was extracted with three portions of $CDCl_3$; all fractions were combined, dried over Na_2SO_4, and analyzed by ^{1}H NMR spectroscopy. The product peak assignments were based on the published data [67], while quantifications

were performed via the integration of the selected peaks of the product and comparison of their intensities with those of the standard.

3.4. Instrumentation

Particle size measurements were performed by dynamic light scattering using a thermally stabilized semiconductor laser with a wavelength of 638 nm on a Photocor Compact-Z particle size analyzer at 25 °C.

The zeta-potential of the particles was measured by the electrophoretic light scattering on a Photocor Compact-Z device with a graphite electrode.

The IR spectra of the compounds were recorded on a Shimadzu IRPrestige 21 Fourier transform IR spectrometer equipped with an MCT detector using a Miracle ATR unit manufactured by Pike.

Differential thermal thermogravimetric analysis (DTA/TG) was performed on an SDT Q600 thermal analyzer (TA Instruments, USA) in the temperature range of 25–80 °C in the dynamic mode. The heating rate was 10°/min. The experiments were carried out in ceramic crucibles.

X-ray analysis of the samples was carried out on a Dron-7 X-ray diffractometer. The 2θ angle interval from 7° to 40° with scanning step Δ2θ = 0.02° and exposure of 7 s per point was used. Cu K_α radiation (Ni filter) was used, which was subsequently decomposed into $K_{\alpha1}$ and $K_{\alpha2}$ components during the processing of the spectra.

X-ray fluorescence analysis of the samples was performed on a Clever C-31 X-ray fluorescence spectrometer. The relative measurement error was ±7%. A rhodium tube with a voltage of 50 kV and a current of 100 μA acted as a generator of γ-rays. The samples were taken without filters for 2000 s.

^{1}H NMR spectra were recorded on a Bruker Advance II spectrometer (Karlsruhe, Germany) operating at a frequency of 400 MHz.

Thin-layer chromatography (TLC) was performed on Merck 60 $F_{254}SiO_2$ plates with a hexane:chloroform 1:1 (v:v) mixture as eluent. Visualization was carried out in ultraviolet light using an HP-UVISfi UV-lamp (Russia).

High-resolution electrospray ionization mass spectrometry (the positive ion mode) was carried out on a Bruker APEX-Qe ESI FT-ICR instrument (USA) with CH_3CN as a solvent.

Inductively coupled plasma-atomic emission spectroscopy measurements were performed with a Leeman ICP-AES Prodigy XP spectrometer.

Elemental analyses were carried out using a Perkin-Elmer elemental analyzer. Degree of succination (DSu) was calculated from elemental analysis data as follows [68]:

$$DSu = \frac{1}{4}[w(C)/w(N)_{succinated\ system} - w(C)/w(N)_{starting\ system}] \times (14/12) \times 100$$

4. Conclusions

Several main aspects of this research can be emphasized:

(i) Indeed, treatment of chitosan (or its cholesterol conjugate) with copper(II) sulfate or acetate, followed by coating with a layer of sodium hyaluronate or succination (if necessary), makes it possible to obtain a wide range of structurally similar systems (Figure 1, Table 1). In addition, we were able to obtain some of these systems in the form of nanoparticles (mainly copper(II) sulfate-based systems), and the second part is a coarse-grained powder (mainly copper(II) acetate-based systems). The molecular weight of the used chitosan practically does not affect the characteristics of the systems obtained;

(ii) Cholesterol-containing systems have proven to be highly efficient catalysts for cross-couplings (Sonogashira, Buchwald–Hartwig, and Chan–Lam); succinated systems coated with a layer of hyaluronic acid are catalysts for the aldol reaction; systems

containing inorganic copper(II) salt nanoparticles are capable of catalyzing the nitrile-oxide-to-nitrile 1,3-dipolar cycloaddition;

(iii) The elaborated catalytic systems efficiently catalyze the mentioned reactions in the greenest solvent available, i.e., water, under aerobic conditions. The studied catalytic reactions proceed selectively, and the isolation of the product does not require column chromatography. The product is separated from the catalyst by simple filtration or centrifugation.

Supplementary Materials: The following supporting information can be downloaded at: https://www.mdpi.com/article/10.3390/catal13010203/s1, Figure S1: ^{1}H NMR spectrum of the product of the model Sonogashira reaction; Figure S2: ^{1}H NMR spectrum of the product of the Buchwald-Hartwig and Chan-Lam reactions; Figure S3: ^{1}H NMR spectrum of the aldol reaction; Figure S4: ^{1}H NMR spectrum of the 1,3-dipolar cycloaddition of nitrile oxides to nitriles.

Author Contributions: Conceptualization, A.P.D. and A.S.K.; methodology, A.P.D. and A.R.E.; software, V.V.R.; validation, A.A.K., A.G.T., and A.S.K.; formal analysis, N.N.L.; investigation, A.P.D.; resources, R.G.; data curation, O.K.; writing—original draft preparation, A.R.E. and O.K.; writing—review and editing, A.G.T.; visualization, V.N.K.; supervision, A.S.K.; project administration, A.S.K.; funding acquisition, A.S.K. and V.N.K. All authors have read and agreed to the published version of the manuscript.

Funding: This paper has been supported in part by the RUDN University Strategic Academic Leadership Program (award no. 025235-2-000, recipient: V.N. Khrustalev). Funding for this research was provided by the Ministry of Education and Science of the Russian Federation (award no. 075-03-2020-223 (FSSF-2020-0017)).

Data Availability Statement: Not applicable.

Conflicts of Interest: The authors declare no conflict of interest.

References

1. Kolcsár, V.J.; Szőllősi, G. Chitosan as a chiral ligand and organocatalyst: Preparation conditions–property–catalytic performance relationships. *Catal. Sci. Technol.* **2021**, *11*, 7652–7666. [CrossRef]
2. El Kadib, A. Chitosan as a Sustainable Organocatalyst: A Concise Overview. *ChemSusChem* **2015**, *8*, 217–244. [CrossRef]
3. Aranaz, I.; Alcántara, A.R.; Civera, M.C.; Arias, C.; Elorza, B.; Heras Caballero, A.; Acosta, N. Chitosan: An Overview of Its Properties and Applications. *Polymers* **2021**, *13*, 3256. [CrossRef]
4. Kritchenkov, A.S.; Egorov, A.R.; Artemjev, A.A.; Kritchenkov, I.S.; Volkova, O.V.; Kiprushkina, E.I.; Zabodalova, L.A.; Suchkova, E.P.; Yagafarov, N.Z.; Tskhovrebov, A.G.; et al. Novel heterocyclic chitosan derivatives and their derived nanoparticles: Catalytic and antibacterial properties. *Int. J. Biol. Macromol.* **2020**, *149*, 682–692. [CrossRef] [PubMed]
5. Kritchenkov, A.S.; Kletskov, A.V.; Egorov, A.R.; Kurasova, M.N.; Tskhovrebov, A.G.; Khrustalev, V.N. Ultrasound and click chemistry lead to a new chitin chelator. Its Pd(II) complex is a recyclable catalyst for the Sonogashira reaction in water. *Carbohydr. Polym.* **2021**, *252*, 117167. [CrossRef] [PubMed]
6. Kritchenkov, A.S.; Egorov, A.R.; Dysin, A.P.; Volkova, O.V.; Zabodalova, L.A.; Suchkova, E.P.; Kurliuk, A.V.; Shakola, T.V. Ultrasound-assisted Cu(I)-catalyzed azide-alkyne click cycloaddition as polymer-analogous transformation in chitosan chemistry. High antibacterial and transfection activity of novel triazol betaine chitosan derivatives and their nanoparticles. *Int. J. Biol. Macromol.* **2019**, *137*, 592–603. [CrossRef]
7. Kritchenkov, A.S.; Egorov, A.R.; Abramovich, R.A.; Kurliuk, A.V.; Shakola, T.V.; Kultyshkina, E.K.; Meza, M.J.B.; Pavlova, A.V.; Suchkova, E.P.; Thuy, G.L.; et al. Water-soluble triazole chitin derivative and its based nanoparticles: Synthesis, characterization, catalytic and antibacterial properties. *Carbohydr. Polym.* **2021**, *257*, 117593. [CrossRef]
8. Egorov, A.R.; Khubiev, O.; Rubanik, V.V.; Rubanik, V.V.; Lobanov, N.N.; Savilov, S.V.; Kirichuk, A.A.; Kritchenkov, I.S.; Tskhovrebov, A.G.; Kritchenkov, A.S. The first selenium containing chitin and chitosan derivatives: Combined synthetic, catalytic and biological studies. *Int. J. Biol. Macromol.* **2022**, *209*, 2175–2187. [CrossRef]
9. Kritchenkov, A.S.; Kurachenkov, A.I.; Egorov, A.R.; Yagafarov, N.Z.; Fortalnova, E.A.; Lobanov, N.N.; Dysin, A.P.; Khomik, A.S.; Khrustalev, V.N. Novel zinc(II)/chitosan-based composite: Ultrasound-assisted synthesis, catalytic and antibacterial activity. *Mendeleev Commun.* **2020**, *30*, 642–644. [CrossRef]
10. Dalpozzo, R.; Mancuso, R. Copper-Catalyzed Synthesis of Coumarins. A Mini-Review. *Catalysts* **2021**, *11*, 1382. [CrossRef]
11. Manna, S. Copper-Catalyzed Diastereo- and Enantioselective Borylative Cyclization. *Catalysts* **2022**, *12*, 734. [CrossRef]
12. Weidlich, T.; Špryncová, M.; Čegan, A. Copper-Catalyzed Reactions of Aryl Halides with N-Nucleophiles and Their Possible Application for Degradation of Halogenated Aromatic Contaminants. *Catalysts* **2022**, *12*, 911. [CrossRef]

13. Kujur, S.; Verma, S.; Pathak, D.D. Development of a Graphene Oxide-Supported N-Heterocyclic Carbene Copper(I) Complex as a Heterogeneous Catalyst for the Selective N-Monoalkylation of Amines. *Catalysts* **2022**, *12*, 1458. [CrossRef]
14. Zelin, J.; Meyer, C.I.; Duarte, H.A.; Marchi, A. A Stable and Reusable Supported Copper Catalyst for the Selective Liquid-Phase Hydrogenation of 5-Hydroxymethylfurfural to 2,5-Bis(hydroxymethyl)furan. *Catalysts* **2022**, *12*, 1476. [CrossRef]
15. Tarahomi, M.; Alinezhad, H.; Maleki, B. Immobilizing Pd nanoparticles on the ternary hybrid system of graphene oxide, Fe_3O_4 nanoparticles, and PAMAM dendrimer as an efficient support for catalyzing sonogashira coupling reaction. *Appl. Organomet. Chem.* **2019**, *33*, e5203. [CrossRef]
16. Laffafchi, F.; Tajbakhsh, M.; Sarrafi, Y.; Maleki, B.; Ghani, M. Cu-Modified Magnetic Creatine as an Efficient Catalyst for Regioselective Preparation of 1,2,3-Triazoles Derivatives. *Polycycl. Aromat. Compd.* **2022**. [CrossRef]
17. Chemler, S.R. Copper catalysis in organic synthesis. *Beilstein J. Org. Chem.* **2015**, *11*, 2252–2253. [CrossRef] [PubMed]
18. Clavadetscher, J.; Hoffmann, S.; Lilienkampf, A.; Mackay, L.; Yusop, R.M.; Rider, S.A.; Mullins, J.J.; Bradley, M. Copper Catalysis in Living Systems and In Situ Drug Synthesis. *Angew. Chem. Int. Ed.* **2016**, *55*, 15662–15666. [CrossRef]
19. Shiri, P. An overview on the copper-promoted synthesis of five-membered heterocyclic systems. *Appl. Organomet. Chem.* **2020**, *34*, e5600. [CrossRef]
20. Shiri, P.; Aboonajmi, J. A systematic review on silica-, carbon-, and magnetic materials-supported copper species as efficient heterogeneous nanocatalysts in "click" reactions. *Beilstein J. Org. Chem.* **2020**, *16*, 551–586. [CrossRef]
21. Ueda, S.; Nagasawa, H. Synthesis of 2-Arylbenzoxazoles by Copper-Catalyzed Intramolecular Oxidative C–O Coupling of Benzanilides. *Angew. Chem. Int. Ed.* **2008**, *47*, 6411–6413. [CrossRef]
22. Jiao, L.-Y.; Zhang, Z.; Hong, Q.; Ning, Z.-H.; Liu, S.; Sun, M.; Hao, Q.; Xu, L.; Li, Z.; Ma, X.-X. Recyclable copper catalyst on chitosan for facile preparation of alkyl/aryl mixed phosphates via deaminated esterification between diphenylphosphoryl azides and aliphatic alcohols. *Mol. Catal.* **2020**, *494*, 111120. [CrossRef]
23. Shen, C.; Xu, J.; Yu, W.; Zhang, P. A highly active and easily recoverable chitosan@copper catalyst for the C–S coupling and its application in the synthesis of zolimidine. *Green Chem.* **2014**, *16*, 3007–3012. [CrossRef]
24. Baig, R.B.N.; Varma, R.S. Copper on chitosan: A recyclable heterogeneous catalyst for azide–alkyne cycloaddition reactions in water. *Green Chem.* **2013**, *15*, 1839–1843. [CrossRef]
25. Williams, A.; Ibrahim, I.T. Carbodiimide chemistry: Recent advances. *Chem. Rev.* **1981**, *81*, 589–636. [CrossRef]
26. Cammarata, C.R.; Hughes, M.E.; Ofner, C.M., III. Carbodiimide Induced Cross-Linking, Ligand Addition, and Degradation in Gelatin. *Mol. Pharm.* **2015**, *12*, 783–793. [CrossRef]
27. Bashir, S.; Teo, Y.Y.; Ramesh, S.; Ramesh, K.; Khan, A.A. N-succinyl chitosan preparation, characterization, properties and biomedical applications: A state of the art review. *Rev. Chem. Eng.* **2015**, *31*, 563–597. [CrossRef]
28. Yanat, M.; Schroën, K. Preparation methods and applications of chitosan nanoparticles; with an outlook toward reinforcement of biodegradable packaging. *React. Funct. Polym.* **2021**, *161*, 104849. [CrossRef]
29. Eremin, D.B.; Ananikov, V.P. Understanding active species in catalytic transformations: From molecular catalysis to nanoparticles, leaching, "Cocktails" of catalysts and dynamic systems. *Coord. Chem. Rev.* **2017**, *346*, 2–19. [CrossRef]
30. Wang, D.; Gao, S. Sonogashira coupling in natural product synthesis. *Org. Chem. Front.* **2014**, *1*, 556–566. [CrossRef]
31. Nagarapu, L.; Karnakanti, S.; Bantu, R. Total synthesis of sapinofuranone A from d-ribose. *Tetrahedron* **2012**, *68*, 5829–5832. [CrossRef]
32. Miller, M.W.; Johnson, C.R. Sonogashira Coupling of 2-Iodo-2-cycloalkenones: Synthesis of (+)- and (−)-Harveynone and (−)-Tricholomenyn A. *J. Org. Chem.* **1997**, *62*, 1582–1583. [CrossRef]
33. Garlaschelli, L.; Magistrali, E.; Vidari, G.; Zuffardi, O. Tricholomenyns A and B, novel antimitotic acetylenic cyclohexenone derivatives from the fruiting bodies of Tricholoma acerbum. *Tetrahedron Lett.* **1995**, *36*, 5633–5636. [CrossRef]
34. Osadchii, S.A.; Shul'ts, E.E.; Vasilevskii, S.F.; Polukhina, E.V.; Stepanov, A.A.; Tolstikov, G.A. Study of alkaloids of the Siberian and Altai flora 13. Synthesis of alkynyllappaconitines. *Russ. Chem. Bull.* **2007**, *56*, 356–360. [CrossRef]
35. Tolstikova, G.T.; Bryzgalov, O.A.; Sorokina, V.I.; Osadchii, A.S.; Shults, E.E.; Dolgikh, P.M.; Khvostov, V.M. Solification with Hydrobromic Acid as a Factor Defining the Antiarrhythmic Effect of Lappaconitine Derivatives. *Lett. Drug Des. Discov.* **2009**, *6*, 475–477. [CrossRef]
36. Magano, J.; Dunetz, J.R. Large-Scale Applications of Transition Metal-Catalyzed Couplings for the Synthesis of Pharmaceuticals. *Chem. Rev.* **2011**, *111*, 2177–2250. [CrossRef] [PubMed]
37. Hervé, G.; Len, C. Heck and Sonogashira couplings in aqueous media—Application to unprotected nucleosides and nucleotides. *Sustain. Chem. Process.* **2015**, *3*, 3. [CrossRef]
38. Mohjer, F.; Mofatehnia, P.; Rangraz, Y.; Heravi, M.M. Pd-free, Sonogashira cross-coupling reaction. An update. *J. Organomet. Chem.* **2021**, *936*, 121712. [CrossRef]
39. Chinchilla, R.; Nájera, C. The Sonogashira Reaction: A Booming Methodology in Synthetic Organic Chemistry. *Chem. Rev.* **2007**, *107*, 874–922. [CrossRef] [PubMed]
40. Chen, J.-Q.; Li, J.-H.; Dong, Z.-B. A Review on the Latest Progress of Chan-Lam Coupling Reaction. *Adv. Synth. Catal.* **2020**, *362*, 3311–3331. [CrossRef]
41. Heravi, M.M.; Kheilkordi, Z.; Zadsirjan, V.; Heydari, M.; Malmir, M. Buchwald-Hartwig reaction: An overview. *J. Organomet. Chem.* **2018**, *861*, 17–104. [CrossRef]
42. Yuan, C.; Zhang, L.; Zhao, Y. Cu(II)-Catalyzed C-N Coupling of (Hetero)aryl Halides and N-Nucleophiles Promoted by α-Benzoin Oxime. *Molecules* **2019**, *24*, 4177. [CrossRef]

43. Zheng, Y.-N.; Zheng, H.; Li, T.; Wei, W.-T. Recent Advances in Copper-Catalyzed C−N Bond Formation Involving N-Centered Radicals. *ChemSusChem* **2021**, *14*, 5340–5358. [CrossRef]
44. Sahoo, H.; Mukherjee, S.; Grandhi, G.S.; Selvakumar, J.; Baidya, M. Copper Catalyzed C–N Cross-Coupling Reaction of Aryl Boronic Acids at Room Temperature through Chelation Assistance. *J. Org. Chem.* **2017**, *82*, 2764–2771. [CrossRef] [PubMed]
45. Mahrwald, R. *Modern Aldol Reactions*; Wiley-VCH Verlag GmbH & Co: Weinheim, Germany, 2004; p. 679.
46. Mukaiyama, T. The Directed Aldol Reaction. In *Organic Reactions*; Wiley: Hoboken, NJ, USA, 1982; pp. 203–331. [CrossRef]
47. Heathcock, C.H. The Aldol Reaction: Acid and General Base Catalysis. In *Comprehensive Organic Synthesis*; Trost, B.M., Fleming, I., Eds.; Pergamon: Oxford, UK, 1991; pp. 133–179.
48. Mestres, R. A green look at the aldol reaction. *Green Chem.* **2004**, *6*, 583–603. [CrossRef]
49. Li, J.J.; Johnson, D.S.; Sliskovic, D.R.; Roth, B.D. *Contemporary Drug Synthesis*; John Wiley & Sons: Hoboken, NJ, USA, 2004; p. 221.
50. Braun, M.; Devant, R.D. (R)- and (S)-2-acetoxy-1,1,2-triphenylethanol—Effective synthetic equivalents of a chiral acetate enolate. *Tetrahedron Lett.* **1984**, *25*, 5031–5034. [CrossRef]
51. Schetter, B.; Mahrwald, R. Modern aldol methods for the total synthesis of polyketides. *Angew. Chem. Int. Ed.* **2006**, *45*, 7506–7525. [CrossRef] [PubMed]
52. Mandal, S.; Mandal, S.; Ghosh, S.K.; Ghosh, A.; Saha, R.; Banerjee, S.; Saha, B. Review of the aldol reaction. *Synth. Commun.* **2016**, *46*, 1327–1342. [CrossRef]
53. Bargujar, S.; Ratnani, S. Aldol condensation: Green perspectives. *J. Iran. Chem. Soc.* **2022**, *19*, 2171–2190. [CrossRef]
54. Breugst, M.; Reissig, H.-U. The Huisgen Reaction: Milestones of the 1,3-Dipolar Cycloaddition. *Angew. Chem. Int. Ed.* **2020**, *59*, 12293–12307. [CrossRef] [PubMed]
55. Himo, F.; Demko, Z.P.; Noodleman, L.; Sharpless, K.B. Why Is Tetrazole Formation by Addition of Azide to Organic Nitriles Catalyzed by Zinc(II) Salts? *J. Am. Chem. Soc.* **2003**, *125*, 9983–9987. [CrossRef]
56. Sommer, M.G.; Rechkemmer, Y.; Suntrup, L.; Hohloch, S.; van der Meer, M.; van Slageren, J.; Sarkar, B. Structural snapshots in the copper(ii) induced azide–nitrile cycloaddition: Effects of peripheral ligand substituents on the formation of unsupported μ1,1-azido vs. μ1,4-tetrazolato bridged complexes. *Dalton Trans.* **2016**, *45*, 17770–17781. [CrossRef]
57. Kuznetsov, M.L.; Kukushkin, V.Y.; Haukka, M.; Pombeiro, A.J.L. 1,3-Dipolar cycloaddition of nitrile oxides to free and Pt-bound nitriles: A theoretical study of the activation effect, reactivity and mechanism. *Inorg. Chim. Acta* **2003**, *356*, 85–94. [CrossRef]
58. *Nitrile Oxides, Nitrones and Nitronates in Organic Synthesis: Novel Strategies in Synthesis*; John Wiley & Sons: Hoboken, NJ, USA, 2008; p. 768.
59. Bokach, N.A.; Kukushkin, V.Y. Coordination chemistry of dialkylcyanamides: Binding properties, synthesis of metal complexes, and ligand reactivity. *Coord. Chem. Rev.* **2013**, *257*, 2293–2316. [CrossRef]
60. Jaleh, B.; Nasrollahzadeh, M.; Nasri, A.; Eslamipanah, M.; Moradi, A.; Nezafat, Z. Biopolymer-derived (nano)catalysts for hydrogen evolution via hydrolysis of hydrides and electrochemical and photocatalytic techniques: A review. *Int. J. Biol. Macromol.* **2021**, *182*, 1056–1090. [CrossRef]
61. Razzaghi, M.; Homaei, A.; Vianello, F.; Azad, T.; Sharma, T.; Nadda, A.K.; Stevanato, R.; Bilal, M.; Iqbal, H.M.N. Industrial applications of immobilized nano-biocatalysts. *Bioprocess Biosyst. Eng.* **2022**, *45*, 237–256. [CrossRef]
62. Dubashynskaya, N.V.; Golovkin, A.S.; Kudryavtsev, I.V.; Prikhodko, S.S.; Trulioff, A.S.; Bokatyi, A.N.; Poshina, D.N.; Raik, S.V.; Skorik, Y.A. Mucoadhesive cholesterol-chitosan self-assembled particles for topical ocular delivery of dexamethasone. *Int. J. Biol. Macromol.* **2020**, *158*, 811–818. [CrossRef] [PubMed]
63. Kritchenkov, A.S.; Luzyanin, K.V.; Bokach, N.A.; Kuznetsov, M.L.; Gurzhiy, V.V.; Kukushkin, V.Y. Selective Nucleophilic Oxygenation of Palladium-Bound Isocyanide Ligands: Route to Imine Complexes That Serve as Efficient Catalysts for Copper-/Phosphine-Free Sonogashira Reactions. *Organometallics* **2013**, *32*, 1979–1987. [CrossRef]
64. Dombrovskii, A.V.; Tashchuk, K.G. Haloarylation of unsaturated compounds by aromatic diazo compounds. XVII. Arylation of α-chlorostyrene and preparation of tolans. *Zh. Obshch. Khim.* **1963**, *33*, 165–170.
65. Astakhov, G.S.; Levitsky, M.M.; Bantreil, X.; Lamaty, F.; Khrustalev, V.N.; Zubavichus, Y.V.; Dorovatovskii, P.V.; Shubina, E.S.; Bilyachenko, A.N. Cu(II)-silsesquioxanes as efficient precatalysts for Chan-Evans-Lam coupling. *J. Organomet. Chem.* **2020**, *906*, 121022. [CrossRef]
66. Kritchenkov, A.S.; Egorov, A.R.; Krytchankou, I.S.; Dubashynskaya, N.V.; Volkova, O.V.; Shakola, T.V.; Kurliuk, A.V.; Skorik, Y.A. Synthesis of novel 1H-tetrazole derivatives of chitosan via metal-catalyzed 1,3-dipolar cycloaddition. Catalytic and antibacterial properties of [3-(1H-tetrazole-5-yl)ethyl]chitosan and its nanoparticles. *Int. J. Biol. Macromol.* **2019**, *132*, 340–350. [CrossRef] [PubMed]
67. Bokach, N.A.; Khripoun, A.V.; Kukushkin, V.Y.; Haukka, M.; Pombeiro, A.J.L. A Route to 1,2,4-Oxadiazoles and Their Complexes via Platinum-Mediated 1,3-Dipolar Cycloaddition of Nitrile Oxides to Organonitriles. *Inorg. Chem.* **2003**, *42*, 896–903. [CrossRef] [PubMed]
68. Skorik, Y.A.; Kritchenkov, A.S.; Moskalenko, Y.E.; Golyshev, A.A.; Raik, S.V.; Whaley, A.K.; Vasina, L.V.; Sonin, D.L. Synthesis of N-succinyl- and N-glutaryl-chitosan derivatives and their antioxidant, antiplatelet, and anticoagulant activity. *Carbohydr. Polym.* **2017**, *166*, 166–172. [CrossRef] [PubMed]